Chapter 3

Evolution of QSO Clustering

3.1 Introduction

In this chapter we present an analysis of various QSO surveys. In particular we look at the clustering properties of four recent QSO samples. Much of the motivation for this analysis has been described in Chapter 1. At present, it is technically impossible to obtain spectra (and therefore redshifts) for large, statistically complete samples of high redshift ($z > 1$) galaxies. However, the statistics of QSO samples can be used to study the Universe at these high redshifts.

We have two entwined problems to resolve: Firstly we need to know how the QSO distribution samples the underlying density field. This relationship can generally be both a function of redshift and scale. We can introduce the concept of *bias* to describe this relation between the observable tracers of large-scale structure (in our case, QSOs) and the density perturbations in the mass distribution. Once this first, highly non-trivial, problem is overcome we can use the statistics of QSO clustering and its evolution over time to constrain cosmological parameters, in particular the density parameter, Ω_0, and the cosmological constant, λ_0. In reality these two problems are closely associated and difficult to separate. We therefore use methods of analysis which allow for both biasing and cosmology.

The first QSO survey to show clustering in a well defined sample was the Durham/AAT QSO survey (Boyle, 1986; Boyle et al., 1990). This showed clustering on scales of $< 10\ h^{-1}$ Mpc (Shanks et al., 1987). A large scale QSO 'supercluster' was found in the CFHT survey of 215 QSOs (Crampton et al., 1985; Crampton et al., 1987; Crampton et al., 1989) at $z = 1.1$ which has dimensions $\simeq 50\ h^{-1}$ Mpc in comoving coordinates. However, no significant clustering was found in the remainder of the survey. Shanks & Boyle (1994) (henceforth SB94), combined the completed Durham/AAT UVX sample (Boyle et al., 1990) with the CFHT survey and the ESO/AAT sample (Boyle et al., 1991; Zitelli et al., 1992) of 83 UVX/colour selected QSOs to obtain statistics on a sample of ~ 700 QSOs, finding significant clustering on scales $< 10\ h^{-1}$ Mpc.

Georgantopoulos (1991) (see also Georgantopoulos & Shanks, 1994), carried out a similar analysis on the low redshift Seyferts in the IRAS Point Source Catalogue (de Grijp et al., 1987) and a 2σ clustering signal was found on scales less than 10 h^{-1} Mpc. Boyle & Mo (1993) obtained clustering statistics for the QSOs at low redshift ($z < 0.2$) in the Einstein Extended Medium Sensitivity Survey (EMSS) but did not find a significant clustering signal at small scales. Both of these low redshift results are consistent with the amplitude of QSO clustering at $z = 1.4$ if there is no evolution of the clustering in comoving coordinates. This previous work suggests only a small amount of evolution from a redshift of $z = 0.1$ to $z = 1.4$ if we can assume that the low and high redshift samples come from the same parent population.

Below we describe the QSO samples that are used in this analysis and then in Section 2.3 discuss in detail the techniques used to calculate the auto-correlation function for QSOs, paying particular attention to the effects of cosmology and estimates of errors. Section 2.4 contains the results obtained from the correlation analysis of the QSO surveys and the rest of the chapter is devoted to interpreting these clustering results, in particular looking at clustering evolution and biasing.

3.2 Data

3.2.1 The QSO samples

The largest of the four surveys used in this analysis is the Large Bright Quasar Survey (LBQS) (Hewett et al., 1995). This consists of 18 United Kingdom Schmidt Telescope (UKST) field areas, each $6^\circ \times 6^\circ$, eleven along the equator ($\delta = 0^\circ$), four in the direction of the Virgo Cluster, and three in the South. QSOs were selected using UKST objective prism plates, and broad band fluxes were obtained from direct plates in the b_J band. Both sets of plates were scanned by the Automatic Plate Measuring (APM) machine. The bright magnitude limit for the survey is $b_J = 16.0$ and the faint magnitude limit varies from field to field in the range $18.41 < b_{J\ \mathrm{lim}} < 18.85$. A conservative error of $\Delta m = 0.15$ (Foltz et al., 1987) is suggested for the QSO magnitudes. Follow-up spectroscopy was obtained from the Multiple Mirror Telescope (MMT) and the Las Campanas Du Pont Telescope. The survey contains a total of 1053 QSOs and their redshift distribution can be seen in Fig. 3.1.

The Durham/AAT QSO survey (Boyle et al., 1990) is a colour selected QSO catalogue, using the Ultra-Violet Excess (UVX) technique. Colours were obtained from COSMOS measurements of eight sets of UKST plates in the b_J and u bands and QSO candidates were selected from their blue $u - b$ colours. The faint limiting magnitude is $b = 21$. Spectroscopy was carried out using the FOCAP system at the Anglo-Australian Telescope (AAT) in 34 $40'$ diameter fields randomly placed within the UKST plate areas. The sample contains 392 QSOs with redshifts in the range

$0.3 < z < 2.2$ (the effective range of the UVX selection technique).

The third survey used is the Canada-France-Hawaii Telescope (CFHT) Survey (Crampton et al., 1989). This is an objective prism/colour selected sample based on four CFHT plate areas. One of the sub-fields within these plate areas may not be representative of the underlying QSO distribution as observations in this field (at $12^{\rm h}48^{\rm m} + 27°$) were concentrated on a previously known QSO 'supercluster' at $z = 1.1$. When considering this survey we will quote results both with and without the region $0.9 < z < 1.2$ in this field included in our analysis (removing this region rejects 30 QSOs from the sample). The faint limit for this survey is $B = 20.5$. At this limit there are 215 QSOs within the same redshift range as the Durham/AAT survey.

Lastly, the ESO/AAT survey (Boyle et al., 1991; Zitelli et al., 1992) is a smaller colour/UVX selected survey using AAT and European Southern Observatory (ESO) 3.6m telescope plates to a fainter limiting magnitude of $B = 22.5$. Spectroscopy was carried out using FOCAP and EFOSC. The sample contains 83 QSOs in the range $0.3 < z < 2.2$.

3.2.2 Comparison of LBQS and other surveys

The LBQS has a considerably brighter magnitude limit than the three other surveys used in this work, which raises particular problems when considering clustering analysis. The number-magnitude relation for QSOs is particularly steep over the range covered by the LBQS and only flattens at $B \simeq 19.15$,

$$n(< B) \propto 10^{0.86B} \ (B < 19.15) \tag{3.1}$$

$$n(< B) \propto 10^{0.28B} \ (B > 19.15) \tag{3.2}$$

(Boyle et al., 1988b). The LBQS therefore has a much lower surface density of QSOs than the three other surveys. At a limiting magnitude of $b_{\rm J} = 18.41$ the LBQS has an effective area of 453.8 deg^2 and 667 QSOs (Hewett et al., 1993) implying a surface density of 1.47 QSOs deg^{-2}. By comparison, the Durham/AAT survey has a surface density of 33.05 QSOs deg^{-2}. The accuracy of the two-point correlation function, $\xi(r)$, defined in Eq. 1.8, is strongly dependent on the number of QSO-QSO pairs at a scale r. It is only when we reach large scales ($\sim 100\ h^{-1}$ Mpc) that the LBQS has more pairs per bin in r than the Durham/AAT sample which is less than twice the size of the LBQS. Thus while at small scales the Durham/AAT, ESO/AAT and CFHT surveys contribute most of the signal, the LBQS is dominant at the largest scales. The shape of the LBQS redshift distribution is also significantly different from that of the other three samples (see Fig. 3.1), peaking at a much lower redshift, so weighting any results towards low redshift. The UVX selection technique can only be used to a redshift of $z = 2.2$, so we shall generally carry out our analysis below this redshift limit.

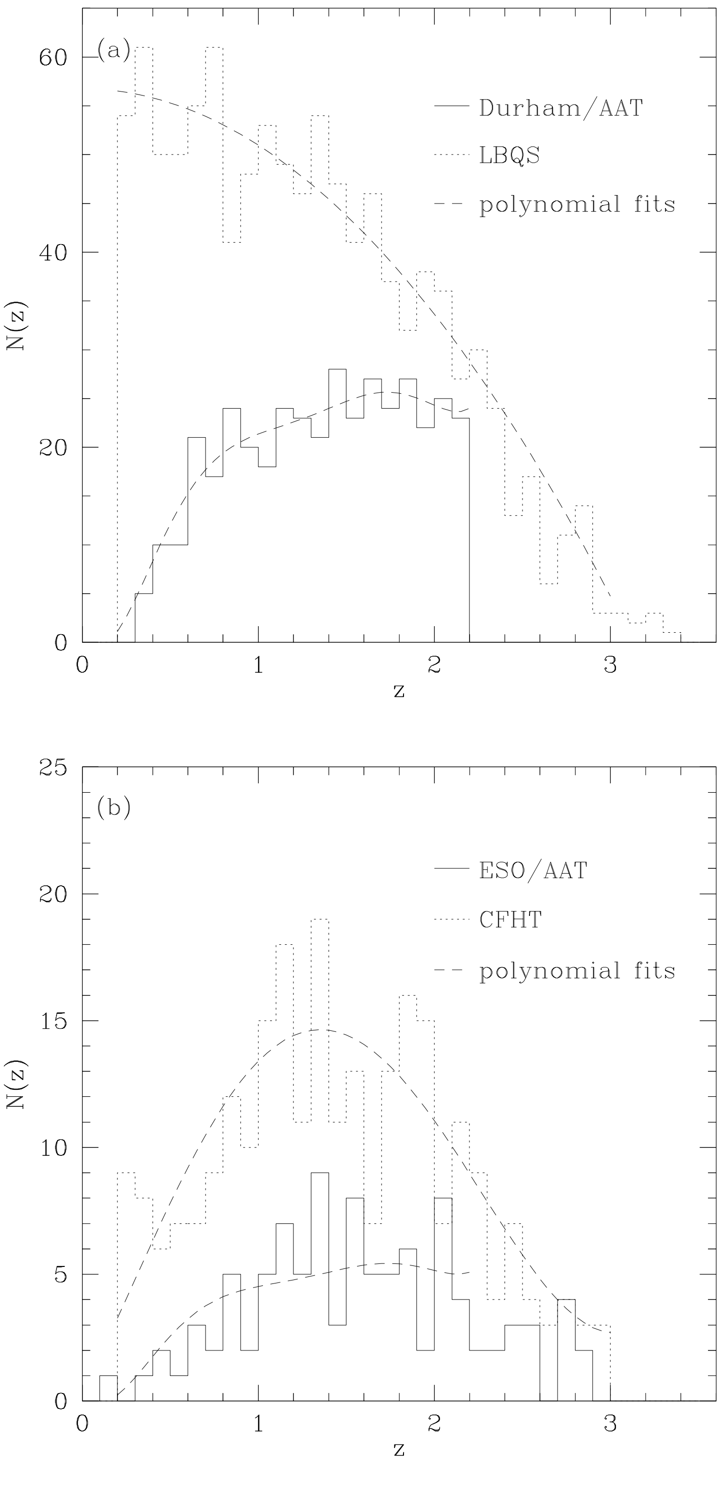

Figure 3.1: The redshift distributions, $N(z)$, for the surveys used in this analysis. (a) The Durham/AAT and LBQS samples, and (b) the CFHT and ESO/AAT samples. Each is plotted with a fitted polynomial, the first three samples using individual fits and the ESO/AAT using a normalized Durham/AAT fit. These polynomials are used in producing the random samples for our calculations of the correlation function.

3.3 Techniques

3.3.1 Correlation function estimates

We use the two-point correlation function as our main estimator of the clustering properties of the above QSO samples. This is defined in Eq. 1.8, but when studying a distribution of point sources rather than a density field this can be defined as

$$\xi(\mathbf{r}) = \langle \delta n(\mathbf{x}+\mathbf{r})\delta n(\mathbf{x})\rangle \tag{3.3}$$

where $n(\mathbf{x})$ is the number density of sources.

On the scales probed with the QSO correlation function, separation is a strong function of cosmology. We use the method of Osmer (1981) which uses the coordinate transformation in the Friedmann-Robertson-Walker metric (Eq. 1.1),

$$\mathbf{X}' = \mathbf{X} + \mathbf{a}[\sqrt{1-k\mathbf{X}^2} - (1-\sqrt{1-k\mathbf{a}^2})(\mathbf{X}.\mathbf{a}/\mathbf{a}^2)] \tag{3.4}$$

(Weinberg, 1972) where $\mathbf{a} = (0, 0, -s_1)$ and $\mathbf{X} = (s_2\sin(\theta), 0, s_2\cos(\theta))$. s_1 and s_2 are the dimensionless comoving distances to QSOs 1 and 2 respectively, and θ is their angular separation on the sky. This is a relatively simple transformation, however, the values s_1 and s_2 depend on the cosmological model used. Taking Eq. 1.1, with $d\tau = 0$ for a photon and assuming the photon travels along a radial path, we have

$$c^2dt^2 = \frac{a^2(t)dr^2}{1-kr^2} \tag{3.5}$$

Integrating this equation from the time of emission of the photon (t_e) to the present (t_0) gives,

$$\int_0^r \frac{\mathrm{d}r}{\sqrt{1-kr^2}} = \int_{t_e}^{t_0} \frac{c\mathrm{d}t}{a(t)} = \int_{a_e}^{a_0} \frac{\mathrm{d}a}{a\dot{a}} \tag{3.6}$$

Writing this equation in terms of redshift (using Eqs. 1.2 and 1.6) we can find the comoving distance to an object with redshift, z. This distance is given by

$$x = \frac{c}{H_0a_0}\int_0^z \frac{\mathrm{d}z}{\sqrt{\Omega_0(1+z)^3 - (\frac{3}{2}\Omega_0 - q_0 - 1)(1+z)^2 + \frac{\Omega_0}{2} - q_0}} \tag{3.7}$$

and

$$s = \begin{cases} \sin(x) & k=1 \\ x & k=0 \\ \sinh(x) & k=-1 \end{cases} \tag{3.8}$$

When we are considering the case of $\lambda_0 = 0$, Eq. 3.7 reduces to

$$x = \frac{c}{H_0a_0}\int_0^z \frac{\mathrm{d}z}{(1+z)\sqrt{\Omega_0 z + 1}} \tag{3.9}$$

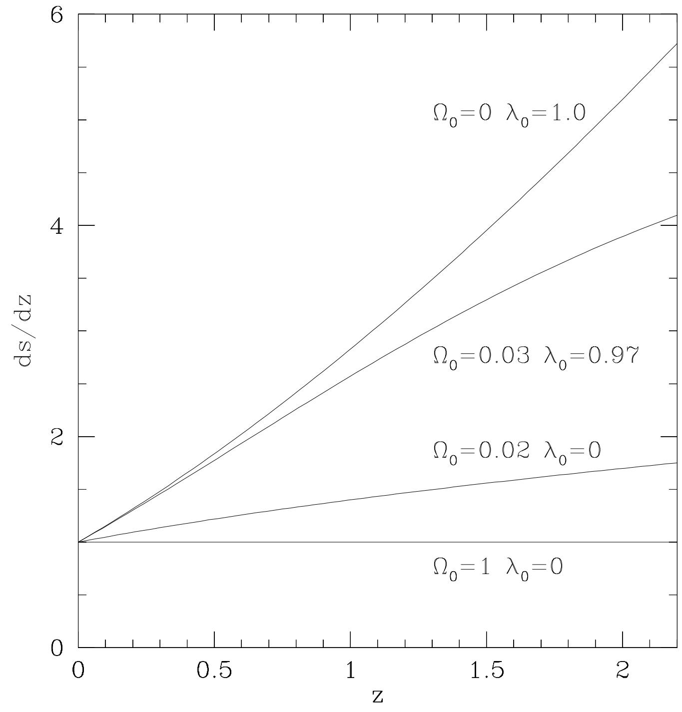

Figure 3.2: $\mathrm{d}s/\mathrm{d}z$ as a function of redshift, normalized to $\mathrm{d}s/\mathrm{d}z$ for $q_0 = 0.5$, where s is the comoving distance. This is plotted for some of the cosmologies used in our analysis, namely $q_0 = 0.5$ and $q_0 = 0.01$ with $\lambda_0 = 0$, and flat low Ω_0 models with $\lambda_0 = 0.97$ and 1.0.

and we can solve exactly, obtaining

$$s = \frac{zq_0 + (q_0 - 1)(\sqrt{2zq_0 + 1} - 1)}{(1 + z)q_0^2} \tag{3.10}$$

For $\lambda_0 \neq 0$ the integral can only be solved numerically, however an approximation (Peebles, 1984) can be used for inflationary (i.e. flat, $k = 0$) Λ models,

$$s = z \text{ for } 1 + z < (\Omega_0^{-1} - 1)^{1/3} \tag{3.11}$$

The correlation function is a difference of two comoving distances, so an assumed cosmology will affect ξ via $\mathrm{d}s/\mathrm{d}z$. In Fig. 3.2 we plot the relative $\mathrm{d}s/\mathrm{d}z$ compared to a $q_0 = 0.5$ universe for a number of different cosmologies. The above approximation for inflationary Λ is only exact for $\Omega_0 = 0$ and $\lambda_0 = 1$. For $\Omega_0 = 0.03$ (with $\lambda_0 = 0.97$) the approximation deviates from the true value by 10 per cent at $z = 1$ and 34 per cent at $z = 2$. In this analysis we shall integrate Eq. 3.7 numerically for $\lambda_0 \neq 0$ cosmologies. The comoving separation is then given by

$$r = \frac{c}{H_0 a_0} \begin{cases} \arcsin(|\mathbf{X}'|) & k = 1 \\ |\mathbf{X}'| & k = 0 \\ \operatorname{arcsinh}(|\mathbf{X}'|) & k = -1 \end{cases} \tag{3.12}$$

We use the following estimator to obtain the two-point correlation function:

$$\xi(r) = \frac{N_{\rm qq}(r)}{N_{\rm qr}(r)} \frac{2n_{\rm r}}{(n_{\rm q}-1)} - 1 \tag{3.13}$$

where $N_{\rm qq}$ is the number of QSO-QSO pairs at a separation $r \pm \delta r/2$ and $N_{\rm qr}$ is the number of QSO-random pairs in the same interval. The $2n_{\rm r}/(n_{\rm q}-1)$ term normalizes the number of randoms to the number of QSOs, $n_{\rm q}$ being the number of QSOs and $n_{\rm r}$ the number of random points. We use $n_{\rm r} = 100n_{\rm q}$ within each field. As the magnitude limits for each LBQS field differ, the number of random points is normalized to the number of QSOs in the individual fields. We give each point a random RA, declination and a random redshift weighted by the overall $N(z)$ for the QSO sample. Other estimators for the two-point correlation function have been suggested, such as

$$\xi(r) = \frac{N_{\rm qq}(r) N_{\rm rr}(r)}{N_{\rm qr}^2(r)} - 1 \tag{3.14}$$

(Hamilton, 1993). These other methods were tested but they were not found to be significantly different from the estimator in Eq. 3.13, which was used as it requires significantly less computational time (as no $N_{\rm rr}(r)$ term is needed).

A comment is required concerning the variable effective area in different LBQS fields. All the LBQS fields cover $5.8° \times 5.8°$. However, each field has different regions removed due to overlapping spectra, step-wedges and bright images (Hewett et al., 1995). We calculate $\xi(r)$ for the LBQS by two different methods, the first is to simply take the $5.8° \times 5.8°$ area (apart from those fields which overlap, where the overlaps are removed from one of the fields) and distribute randoms within this region with no regard to any holes in the effective area. The second is to use the real positions of the LBQS QSOs for our random points, but randomly shuffle their redshifts. We then use 1000 realisations of this process to obtain a mean number of QSO-random pairs. When we compare the two processes we find no significant difference; the r.m.s.difference between the two estimates is 0.26σ where σ is the error on the first estimator. This is not altogether unexpected as the LBQS survey regions are much more extended in the radial direction than in the angular direction. Holes in the field would only be expected to contribute to any signal at large scales, and at large scales the redshift component of the distance dominates the signal. Throughout this analysis we will use the first estimator as this should give a less biased estimate of clustering on small scales.

No correlation between fields is attempted, as any systematic magnitude calibration error between fields would mean a considerable QSO density variation. If we use a form for the bright counts such that $N(<B) \propto 10^{0.8B}$ then a ~ 0.1 mag error in the zero point magnitude produces a 20 per cent variation in the QSO surface density. Our normalization is such that it forces the integral correlation function to zero on the very largest scales probed. On small scales we also use the integrated correlation function, $\bar{\xi}(r)$, where

$$\bar{\xi}(r) = \frac{3}{r^3} \int_0^r \xi(x) x^2 {\rm d}x \tag{3.15}$$

To estimate this we simply use the same estimator in Eq. 3.13, but for pairs at separation 0 to r.

3.3.2 Error analysis

Field-to-field variation of number density

We look at the field-to-field variance of the number of QSOs in the LBQS, taking the 18 fields and considering the number counts of QSOs to a limiting magnitude of $b_J = 18.41$ mag. A χ^2 test is carried out on the hypothesis that the fields are derived from the same population. The result is $\chi^2 = 33.92$ for 17 degrees of freedom, which is a rejection of the hypothesis at a 99 per cent significance level. Most of this variation comes from three fields, two equatorial, $01^{\mathrm{h}}00^{\mathrm{m}}\ 00°00'$, $22^{\mathrm{h}}40^{\mathrm{m}}\ 00°00'$, and one southern, $00^{\mathrm{h}}53^{\mathrm{m}}\ -28°00'$, with 56, 24 and 57 QSOs respectively. Without these fields a χ^2 test gives $\chi^2 = 16.47$ on 14 degrees of freedom, only significant at the 70 per cent level. A possible cause of this effect could be residual magnitude errors after calibration, although CCD sequences were used to obtain zero-points and linearize the APM magnitudes. Hewett et al., (1995) suggests that there could still be systematic variations across individual fields of up to 0.1 mag. This justifies our decision not to correlate QSOs between individual fields.

Correlation function errors

Analysis of errors in the two-point correlation function is an area of some debate. In the case of QSOs we have the particular problem that at small scales there are only a small number of pairs, while at the largest scales we can probe, $\xi(r)$ has an intrinsically lower amplitude causing any signal to be close to the noise. To determine our errors, particularly on larger scales, we have carried out an analysis of several different error estimators to find the most accurate and consistent errors for our estimates of the QSO $\xi(r)$. We consider Poisson errors, field-to-field errors, simulations and bootstrap methods (Barrow et al., 1984) to produce estimates for the error on the QSO correlation function.

The Poisson noise due to the number of pairs in the sample is

$$\Delta\xi = \frac{1+\xi}{\sqrt{N_{\mathrm{qq}}}} \tag{3.16}$$

This estimate should be valid at small scales if the signal is still relatively low. The number of pairs is small so most pairs are independent and contribute independent information to the correlation function. At large scales QSO pairs become less independent, and one might expect that n_{q} would be a more realistic error estimate than N_{qq}.

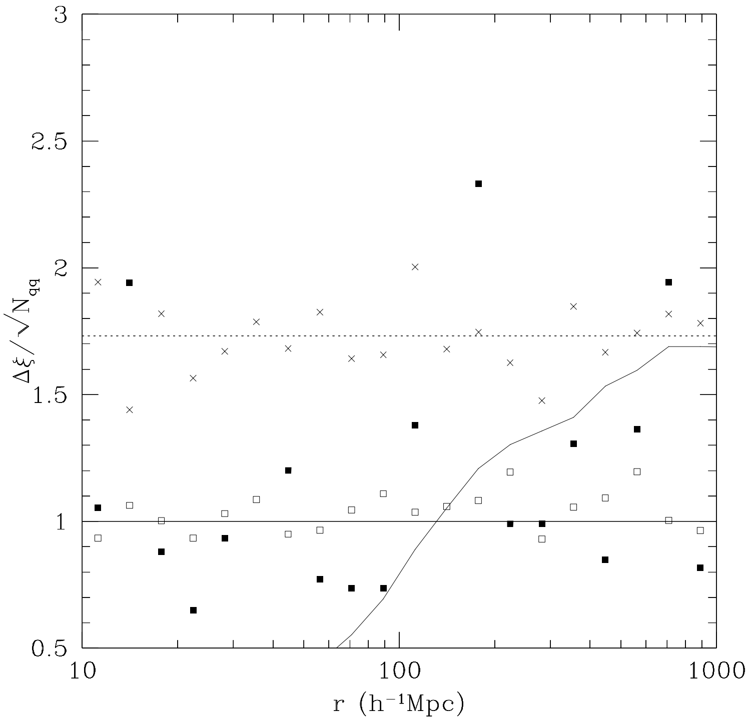

Figure 3.3: Relative estimates of the errors in the 2-point correlation function from simulations (open squares), field-to-field variation (filled squares), bootstrap re-sampling (crosses), and $n_{\rm q}^{1/2}$ (solid line), normalized to $N_{\rm qq}^{1/2}$ for the LBQS sample. The dotted line is $\Delta\xi = (3N_{\rm qq})^{1/2}$, the expected relative error from bootstrap estimates.

For field-to-field errors we have split the LBQS survey up into five regions, each containing ~ 170 QSOs, calculating the variance between these five different correlation function estimates. We produced multiple random (a good approximation to the survey due to the small number of correlated pairs) simulations of the LBQS survey region and found the variance from the estimates of $\xi(r)$ from these simulations. The bootstrap re-sampling was carried out by randomly selecting a sample of n QSOs from a total of n QSOs *with replacement.* For both the simulations and bootstrap re-sampling 100 realisations were used.

In Fig. 3.3 we plot the error estimates normalized to the Poisson ($\sqrt{N_{\rm qq}}$) error for the LBQS sample. The field-to-field variance has a large scatter over all scales probed by the LBQS $\xi(r)$, but $\Delta\xi_{\rm field-field}$ is approximately consistent with $\sqrt{N_{\rm qq}}$ at all these scales. The variance calculated from simulations is also consistent with Poisson errors on all scales. The errors resulting from the bootstrap method are 1.7 times larger than the $\sqrt{N_{\rm qq}}$ at all scales. This is consistent with a suggested analytical expression for the bootstrap error (Mo et al., 1992),

$$\sigma^2_{\rm boot}(r) \simeq 3N_{\rm qq}(r) + \frac{4N^2_{\rm qq}(r)}{n_{\rm q}} \tag{3.17}$$

This expression was formulated assuming a large contiguous region in which the edge effects are negligible. This is obviously not the case for any of the QSO surveys.

As a result the second term in the above expression is always small, particularly as there is no attempt to correlate QSOs between fields. Hence $\Delta\xi_{\rm boot}/\sqrt{N_{\rm qq}} \simeq \sqrt{3}$ at all scales.

At small scales we know that the bootstrap errors overestimate the true errors (Mo et al., 1992). We should therefore use $\sqrt{N_{\rm qq}}$ errors on these scales as they are consistent with both field-field and simulation errors. On larger scales ($> 100\ h^{-1}$ Mpc) the choice is not so obvious. Bootstrap errors should be more realistic on these scales but still overestimate the field-to-field and simulated errors by a factor of $\sqrt{3}$. $n_{\rm q}$ errors are consistent with $N_{\rm qq}$ errors at $\sim 100\ h^{-1}$ Mpc and consistent with bootstrap estimators at $\sim 1000\ h^{-1}$ Mpc. For these reasons (and because of the large amount of time needed to run simulations for every case) the correlation function for the QSOs will be plotted using $\sqrt{N_{\rm qq}}$ errors until $N_{\rm qq} = n_{\rm q}$, then with $\sqrt{n_{\rm q}}$ at larger scales. It should be noted that the majority of our analysis will be carried out below 50 h^{-1} Mpc and in this region it is clear that $\sqrt{N_{\rm qq}}$ is the best choice. When looking for low amplitude signals at larger scales the simulations will be used to obtain a reliable estimate of the uncertainty.

3.4 Results at Small Scales

Correlation functions out to $r = 100\ h^{-1}$ Mpc are shown in Fig. 3.4. Figs. 3.4a and 3.4b show the correlation functions for LBQS and Durham/AAT on log-log plots for $q_0 = 0.5$. The LBQS in particular does not have a strongly significant signal at small scales due to the small number of QSO-QSO pairs at $< 10\ h^{-1}$ Mpc (only five) in the survey. Within the large errors the two surveys both appear to be consistent with the power law,

$$\xi(r) = \left(\frac{r}{r_0}\right)^{-\gamma} \tag{3.18}$$

with $r_0 = 6\ h^{-1}$ Mpc and $\gamma = 1.8$. A χ^2 test on the hypothesis that the data fit this power law gives $\chi^2 = 6.852$ (6 degrees of freedom) and $\chi^2 = 1.608$ (4 degrees of freedom) for the Durham/AAT and LBQS samples respectively, hence the probabilities of the hypothesis being rejected are small, 0.665 and 0.193. This test was carried out below 30 h^{-1} Mpc. The pair-weighted combined QSO $\xi(r)$ for the ESO/AAT and CFHT samples is plotted in Fig. 3.4c. This plot is corrected from the previous version in SB94, which contained an error producing more small scale power and an anti-correlation on scales of $\sim 40 - 100\ h^{-1}$ Mpc. The corrected version of this plot shows excess power over that expected from the $r_0 = 6\ h^{-1}$ Mpc power law at the 30 h^{-1} Mpc scale. This excess power is from the QSO 'supercluster' in the CFHT sample. When the region around the 'supercluster' is removed, the data are consistent with the above power law. Fig 3.4d shows the four surveys combined, using a simple pair weighting. The errors are obtained from Eq. 3.16 and are significantly improved by combining the data. It is possible to find a best fit power law to these data, using a minimum χ^2 fit. For $q_0 = 0.5$ the best fit (without

Table 3.1: The integrated QSO clustering, $\bar{\xi}$, within 10 h^{-1} Mpc and 25 h^{-1} Mpc, for the LBQS and for all surveys combined (excluding the CFHT 'supercluster'). The results are listed for various cosmologies.

Ω_0	$\lambda_\circ$	LBQS $\bar{\xi}(10)$	All $\bar{\xi}(10)$	All $\bar{\xi}(25)$
1	0	1.86 ± 1.28	0.83 ± 0.29	0.16 ± 0.08
0.1	0	1.06 ± 1.45	1.09 ± 0.47	0.21 ± 0.11
0.02	0	1.09 ± 1.48	1.01 ± 0.50	0.28 ± 0.12
0.2	0.8	2.42 ± 2.42	1.01 ± 0.58	0.35 ± 0.14
0.03	0.97	1.54 ± 2.55	0.76 ± 0.79	0.74 ± 0.23

the CFHT 'supercluster') is $r_0 = 4.00 \pm 1.14$ and $\gamma = 1.59 \pm 0.46$ ($r_0 = 4.96 \pm 1.13$ and $\gamma = 1.40 \pm 0.30$ with the CFHT 'supercluster'), (see Fig. 3.4d). The fit is made between the scales 2 and 32 h^{-1} Mpc. It should be noted that varying the range of scales over which this fit is made makes a considerable difference to the best fit parameters, demonstrating that a significantly larger sample is required to obtain a robust result.

Another measure of the clustering amplitude on small scales is the value $\bar{\xi}(r)$ (Eq. 3.15). We calculate this at two scales, $r = 10$ h^{-1} Mpc and $r = 25$ h^{-1} Mpc, the results of this are shown in Table 3.1. Shanks & Boyle (1994) find $\bar{\xi}(10\ h^{-1}\ \mathrm{Mpc}) = 0.93 \pm 0.34$ for Durham/AAT, CFHT (without cluster) and ESO/AAT combined. With the corrected analysis for CFHT and ESO/AAT this becomes $\bar{\xi}(10) = 0.74 \pm 0.30$. For the LBQS individually, $\bar{\xi}(10) = 1.86 \pm 1.28$ (there are only 5 QSO-QSO pairs within 10 h^{-1} Mpc), and combining this with the other surveys, $\bar{\xi}(10) = 0.83 \pm 0.29$. These results and those for other cosmologies are shown in Table 3.1.

Formally the significance of a rejection of a Poisson random distribution is 3.8σ (by comparing 39 pairs found to 21.3 expected). In cosmologies with low Ω_0, we generally find a higher amplitude but larger errors, as pairs move out to larger scales. For $q_0 = 0.01$, $\bar{\xi}(10) = 1.01 \pm 0.50$ (considering the whole sample without the CFHT cluster) and for $\Omega_0 = 0.2$ and $\lambda_0 = 0.8$ we find $\bar{\xi}(10) = 1.01 \pm 0.58$, representing a formal detection of clustering at the 2.8σ and 2.5σ levels respectively.

If the sample ($q_0 = 0.5$) is split into redshift bins then for $0.3 < z < 1.4$, $\bar{\xi}(10) = 0.97 \pm 0.43$ and for $1.4 < z < 2.2$, $\bar{\xi}(10) = 0.68 \pm 0.40$. Although the high redshift signal is lower there is no significant evolution between the two redshift bins. Similarly, the best fit power laws for the low and high redshift bins respectively are $r_0 = 4.48 \pm 1.36$, $\gamma = 2.00 \pm 0.92$ and $r_0 = 4.08 \pm 2.27$, $\gamma = 1.32 \pm 0.60$ which show that although the high redshift correlation function appears to be lower it is not significantly so.

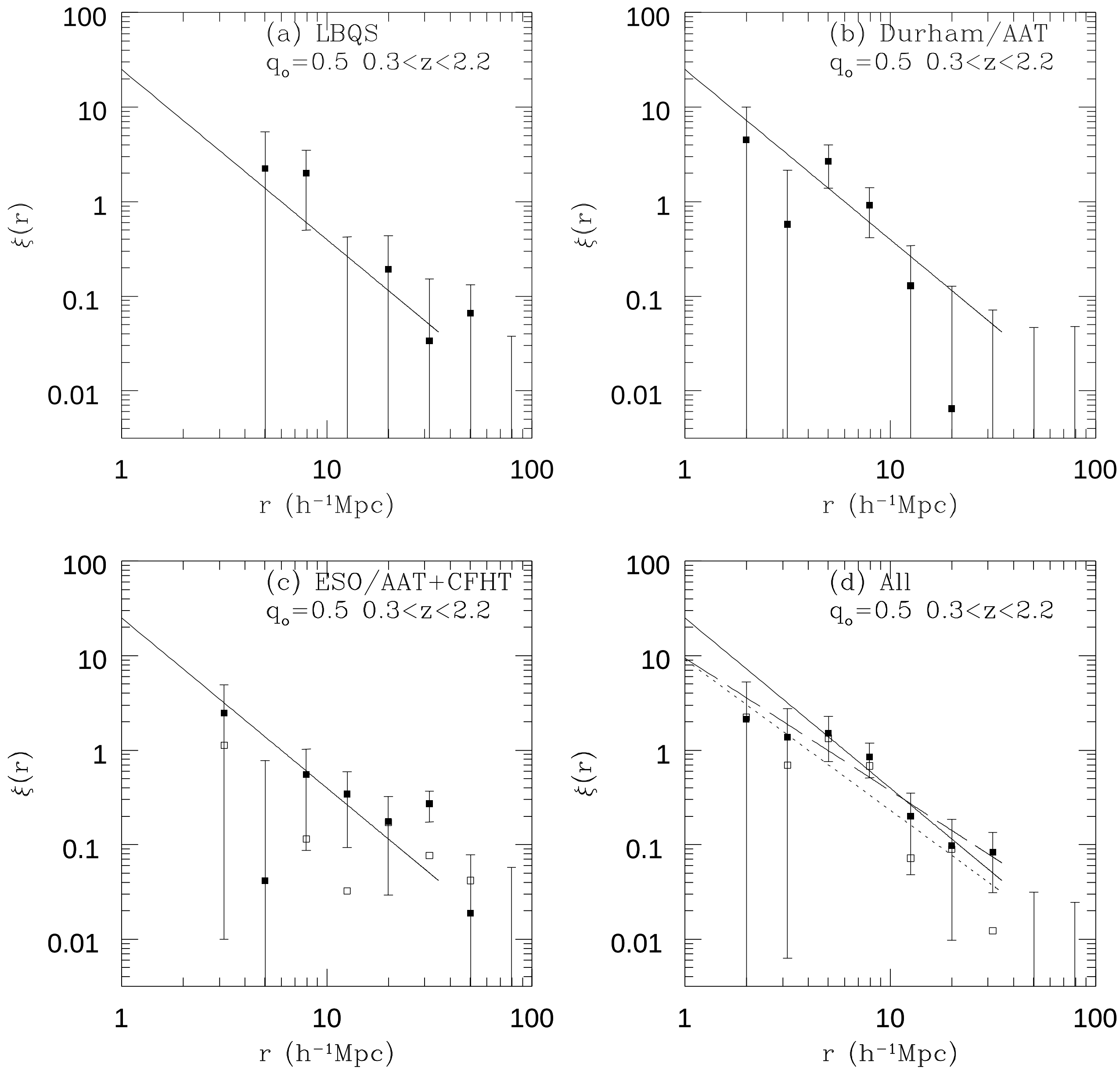

Figure 3.4: QSO correlation functions on small scales for $\Omega_0 = 1.0$ in the redshift range $0.3 < z < 2.2$. (a) The LBQS, (b) the Durham/AAT sample, (c) the corrected ESO/AAT and CFHT combined (open squares with the redshift range $0.9 - 1.2$ removed in the $12^h48^m + 27°$ field) and (d) all surveys combined (again the open symbols are with the CFHT 'supercluster' removed). The solid line in all the plots is a power law with $r_0 = 6\ h^{-1}$ Mpc and $\gamma = 1.8$. Dashed and dotted lines in (d) are the best fit power laws with and without the CFHT 'supercluster' respectively. The data is binned with $\Delta\log(r) = 0.2$.

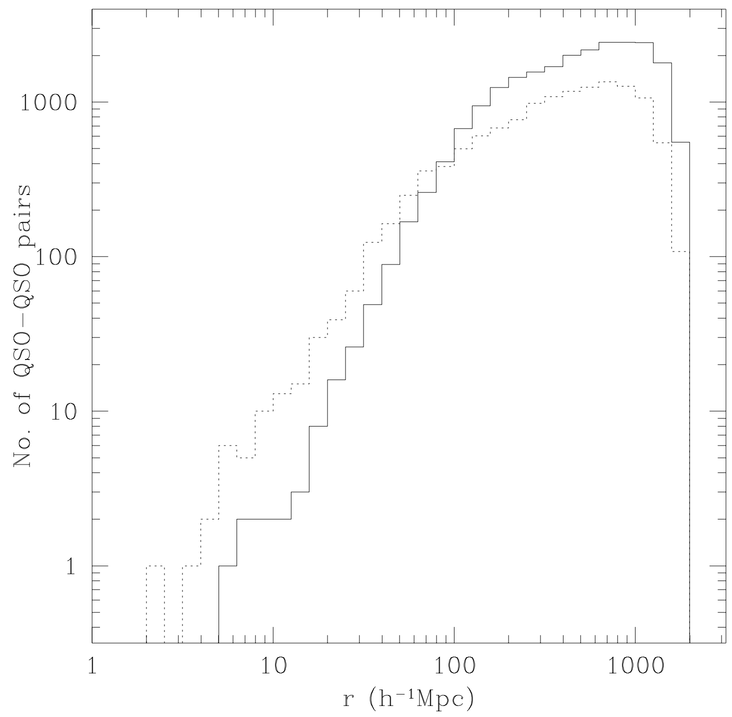

Figure 3.5: The number of QSO-QSO pairs as a function of scale (for $\Omega_0 = 1$) for the LBQS (solid line) and the Durham/AAT sample (dotted line).

3.5 Results at Large Scales

3.5.1 Clustering in the LBQS at large scales

Below we present the results of QSO clustering analysis at larger scales ($r > 20\ h^{-1}$ Mpc). The combined QSO sample of the LBQS, Durham/AAT, CFHT and ESO/AAT surveys gives a total of over 1500 QSOs between $z = 0.3$ and $z = 2.2$.

In Section 3.4 it was pointed out that the LBQS makes very little contribution to clustering statistics on scales less than $\sim 10\ h^{-1}$ Mpc. However, on larger scales the LBQS is an important new probe of structure. The count of QSO pairs peaks at around $800 - 900\ h^{-1}$ Mpc and Fig. 3.5 shows this pair distribution as a function of scale (for $0.3 < z < 2.2$). The Durham/AAT survey has a higher pair count below $100\ h^{-1}$ Mpc, but above this scale the LBQS starts to dominate the signal.

First, we have calculated $\xi(r)$ for the LBQS over the entire redshift range of the sample, $0.2 < z < 3.4$ (Fig. 3.6). This will actually be heavily weighted towards low redshift due to the shape of the LBQS number-redshift relation. The LBQS does not show a significant deviation from $\xi = 0$ on any scale probed, and at scales larger than $100\ h^{-1}$ Mpc the error on $\xi(r)$ is only ± 0.03. In order to compare the LBQS to the other samples we have also calculated $\xi(r)$ for the LBQS in the range $0.3 < z < 2.2$. This is shown in Fig. 3.7a, again there is no significant signal at these large scales.

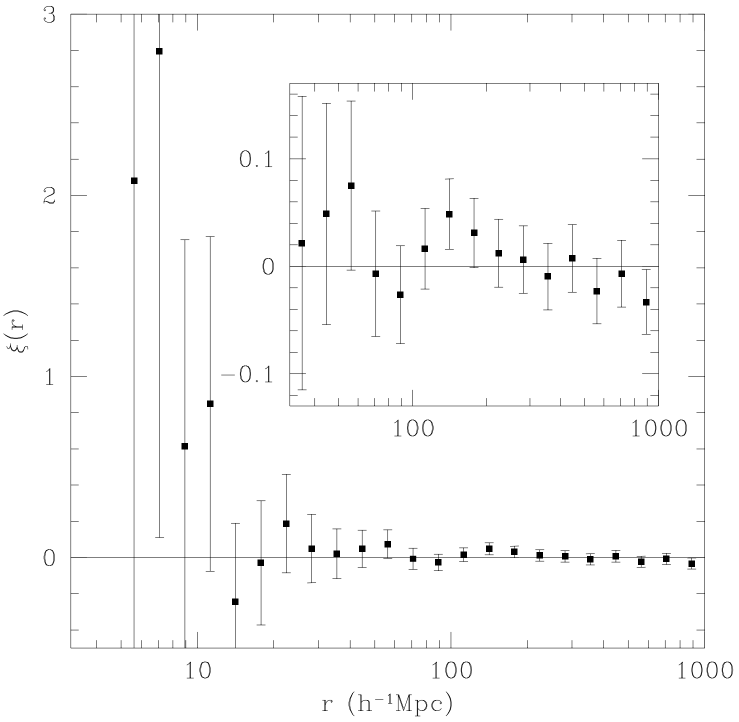

Figure 3.6: The two-point correlation function for the LBQS in the redshift range $0.2 < z < 3.4$. Inset is an expanded version of the plot from 30 to 1000 h^{-1} Mpc. The bins have width $\Delta \log(r) = 0.1$.

Results from the Durham/AAT, ESO/AAT and CFHT are also shown on this plot. Shanks & Boyle (1994) show an anti-correlation in the Durham/AAT survey on scales $40 - 100$ h^{-1} Mpc, significant at the 2σ level, which is not seen in the LBQS. The signal in the Durham/AAT sample is $\xi(40 - 100\ h^{-1}\ \mathrm{Mpc}) = -0.084 \pm 0.036$ (SB94) with errors from simulations. The corresponding signal in the LBQS is $\xi(40 - 100\ h^{-1}\ \mathrm{Mpc}) = 0.00 \pm 0.034$, again using errors from simulations. These two values are consistent at the 2σ level. The revised $\xi(r)$ for the CFHT and ESO/AAT samples also show no anti-correlation on these scales: $\xi(40 - 100\ h^{-1}\ \mathrm{Mpc}) = -0.006 \pm 0.041$. Therefore there is no evidence in the LBQS, CFHT or ESO/AAT samples to support the claimed anti-correlation of Shanks & Boyle (1994), although the difference between the surveys is not strongly significant.

Next, the LBQS was split into redshift bins. For consistency we used the same bins as used by SB94, that is $0.3 < z < 1.4$ and $1.4 < z < 2.2$. The correlation functions for these are shown in Fig. 3.7b. In the $0.3 < z < 1.4$ case there are 556 QSOs, and no significant deviations from zero are seen at any scale. By contrast, in the Durham/AAT sample the anti-correlation seen at $40 - 100$ h^{-1} Mpc is seen largely in the lower redshift range. The high redshift sub-sample of the LBQS shows only one point that significantly deviates from zero. The lack of significant deviations from $\xi = 0$ at large scales is a strong constraint on the inhomogeneity of the Universe.

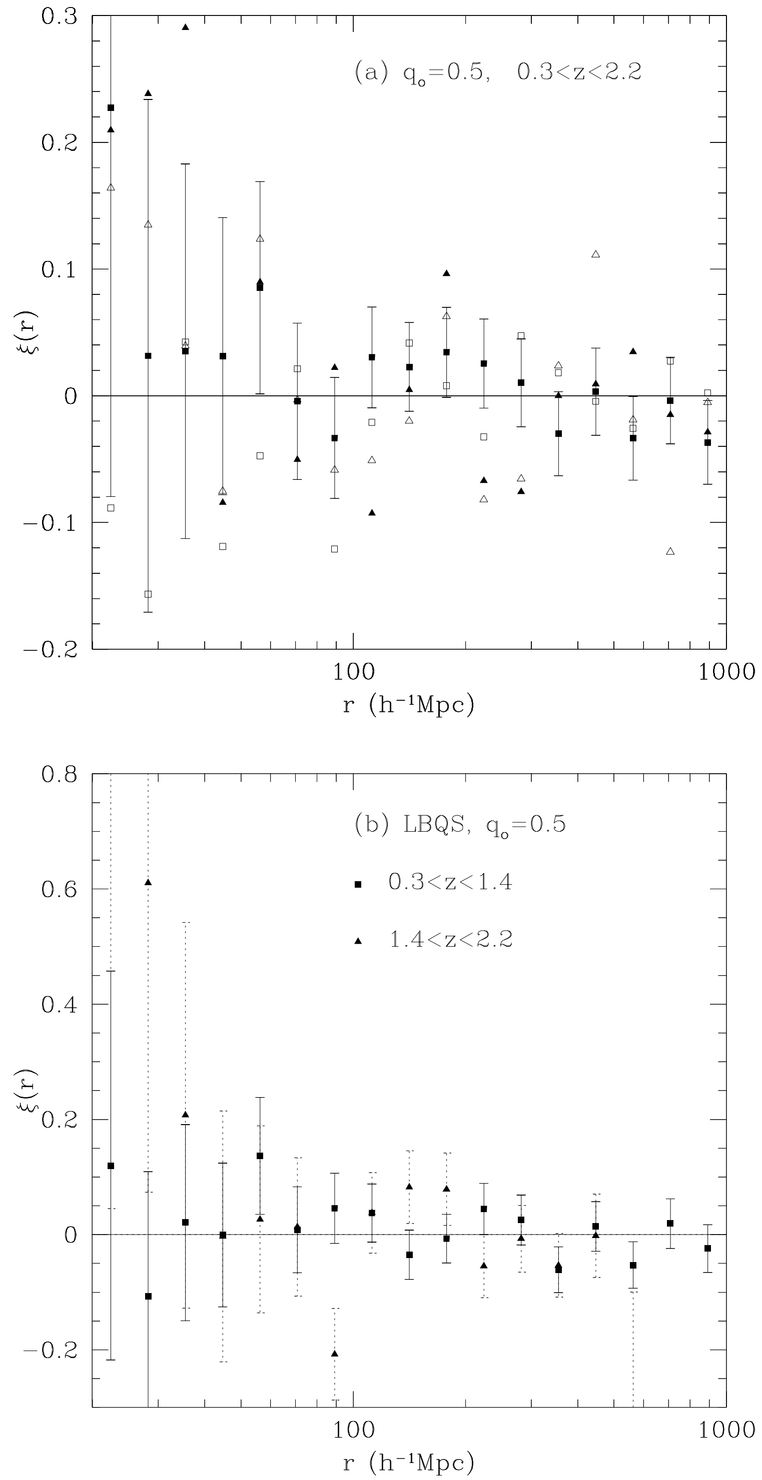

Figure 3.7: QSO Correlation functions with $q_0 = 0.5$ and $0.3 < z < 2.2$. (a) the LBQS (filled squares with errors), Durham/AAT (open squares) and re-analysed CFHT and ESO/AAT (filled triangles, open triangles with CFHT 'supercluster' removed). (b) $\xi(r)$ for LBQS in redshift bins $0.3 < z < 1.4$ (filled squares) and $1.4 < z < 2.2$ (filled triangles).

3.5.2 Large-scale structure in the combined sample of QSOs

The $\xi(r)$ for the combined sample at large scales is shown in Fig. 3.8a, and constitutes one of the most accurate available representations of large-scale structure on scales in excess of 50 h^{-1} Mpc. Removing the CFHT 'supercluster' makes little difference on scales > 30 h^{-1} Mpc. In the region at $40 - 100$ h^{-1} Mpc that caused interest in the Durham/AAT sample, the mean correlation function is now $\xi(40-100\ h^{-1}\ \mathrm{Mpc}) = -0.026 \pm 0.022$ (this error is obtained from simulations, note that $\sqrt{n_\mathrm{q}}$ would give a similar error, ± 0.024). Looking more closely at the region around 100 h^{-1} Mpc there are points at 89 and 177 h^{-1} Mpc that are marginally ($1.5 - 2\sigma$) non-zero, so only tentative evidence of a feature on this scale. Positive signals near these scales have been seen in pencil-beam galaxy surveys (Broadhurst et al., 1990), and it should be remembered that all the QSO surveys are effectively pencil beams, so there is some observational precedent for a signal of this kind. On scales greater than 200 h^{-1} Mpc there are no deviations away from a Poisson distribution. Splitting the combined sample into redshift bins, Fig. 3.8b, we see that both redshift bins contribute to the signal at ~ 100 h^{-1} Mpc but no distinctive features are seen. In the combined sample, we therefore have even tighter constraints on inhomogeneity in the Universe. The upper limits at $r > 100$ h^{-1} Mpc are at the ~ 0.025 level.

Galaxy redshift surveys show impressive amounts of structure when the galaxy distribution is mapped out (e.g. Ratcliffe 1996) . This produces a significant signal in the correlation function at scales of $\sim 20 - 30$ h^{-1} Mpc, as demonstrated by the Durham/UKST Galaxy Redshift Survey (Ratcliffe et al., 1997), the Las Campanas Galaxy Redshift Survey (Tucker et al., 1997) and others. The galaxy auto-correlation functions for these two surveys are compared to the QSO auto-correlation function in Fig. 3.9. The Las Campanas data are consistent with the QSO data while the Durham/UKST result has a slightly higher amplitude on large scales. We should, of course, remember that galaxy clustering measurements are at $z \sim 0$ while the QSOs have a mean redshift of $\bar{z} = 1.27$. Nevertheless, the similarities between the galaxies and QSOs are clear.

3.5.3 QSO $\xi(r)$ in low q_0 and $\Lambda \neq 0$ models

The combined QSO correlation functions for $q_0 = 0.01$ ($\lambda_0 = 0$) and $\Omega_0 = 0.03$, $\lambda_0 = 0.97$ are shown in Fig 3.10. Fig. 3.2 has shown how the differential comoving distance varies with cosmology. This effect can be used to discriminate between cosmologies if it is possible to observe linear features in the correlation function at low redshift. Linear theory predicts that features should not change scale as they evolve, their only evolution being in amplitude. Hence, if a linear feature is observed at low redshift in the correlation function then a corresponding feature should be observable at high redshift, only if the correct cosmology is assumed. Effectively we are using features in the correlation function as standard rods. Both low q_0 and positive Λ increase the average separation between pairs of QSOs.

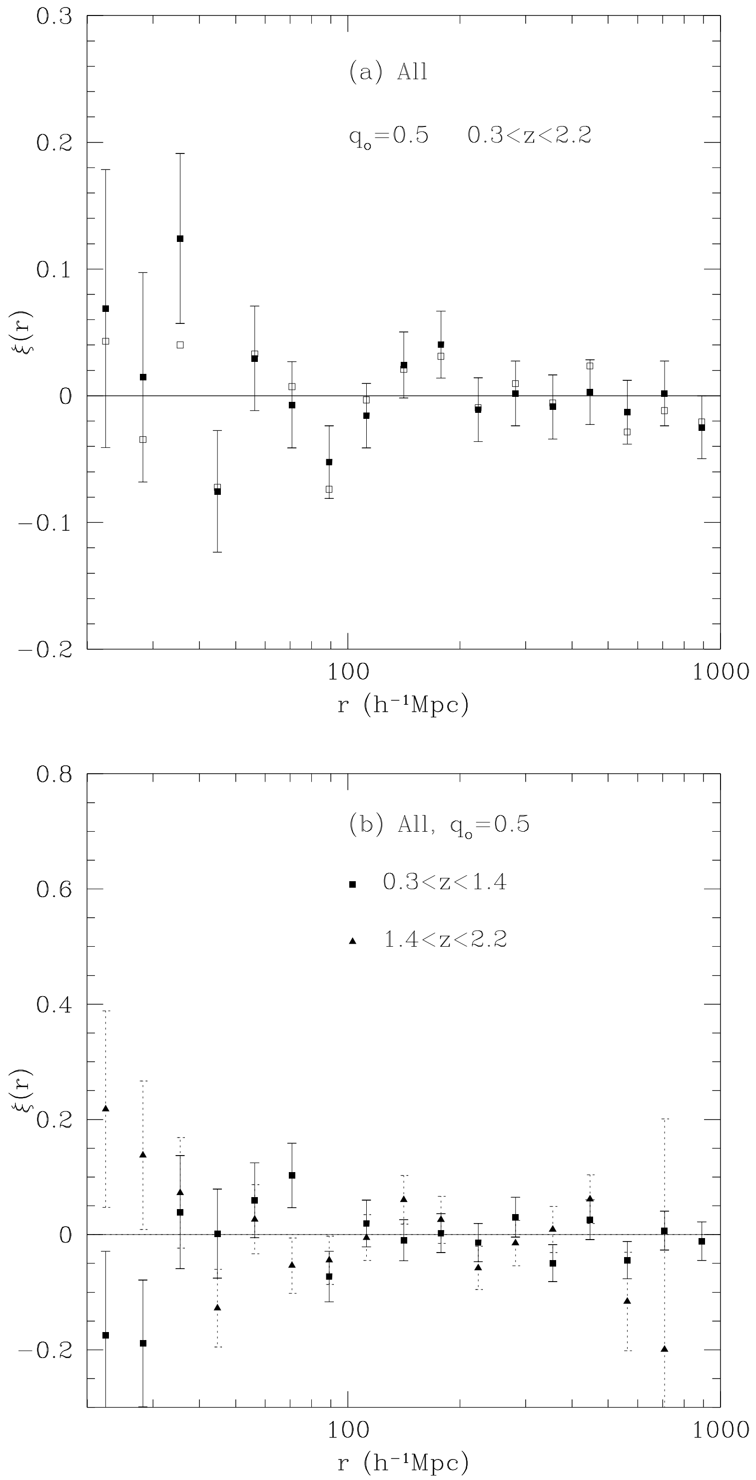

Figure 3.8: The QSO correlation function for the combined sample at large scales, for $q_0 = 0.5$. (a) Redshift range $0.3 < z < 2.2$ (open squares with the CFHT 'supercluster' removed), (b) $0.3 < z < 1.4$ without CFHT 'supercluster' (filled squares) and $1.4 < z < 2.2$ (filled triangles).

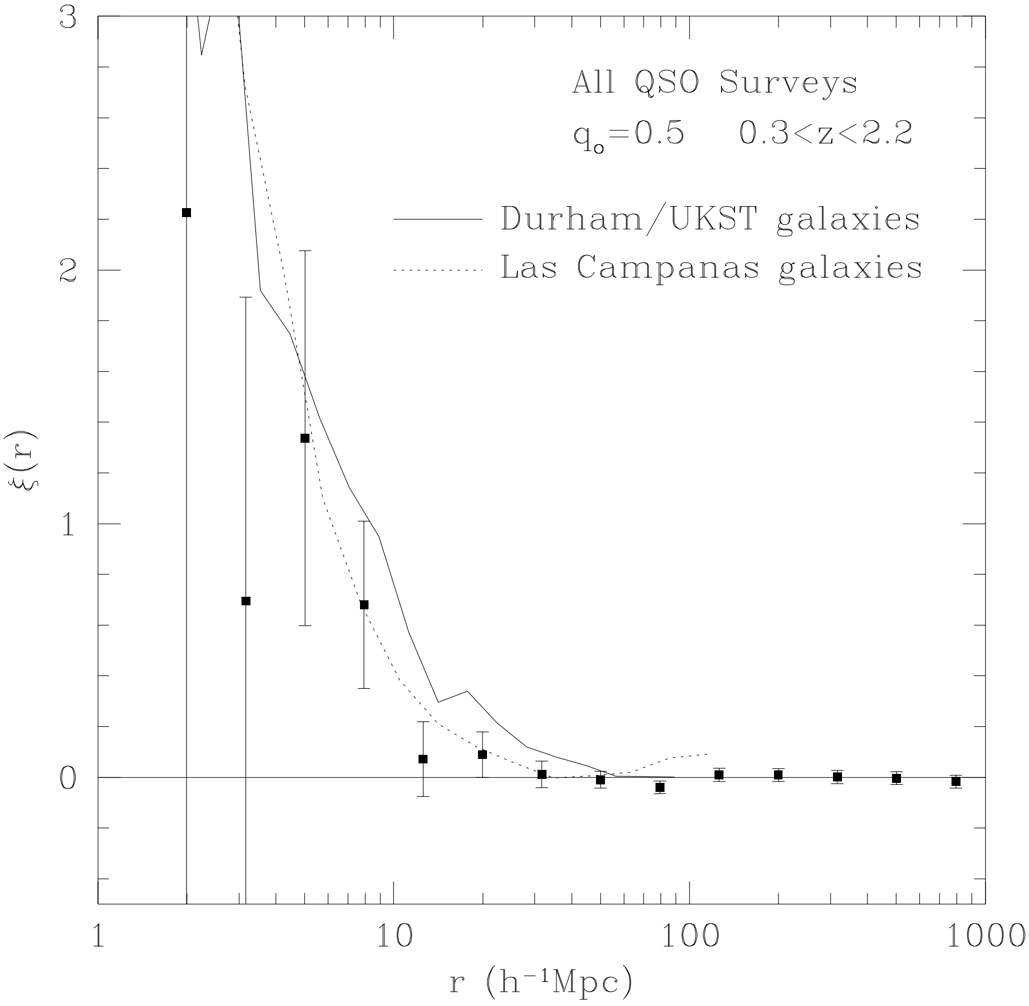

Figure 3.9: The QSO correlation function for the combined sample (with $q_0 = 0.5$ and $0.3 < z < 2.2$) over the entire range of scales probed. The data are binned with $\Delta\log(r) = 0.2$. For clarity only the data without the CFHT 'supercluster' are used. The data are compared to local galaxy correlation functions from the Durham/UKST Redshift Survey (solid line) and the Las Campanas Redshift Survey (dotted line).

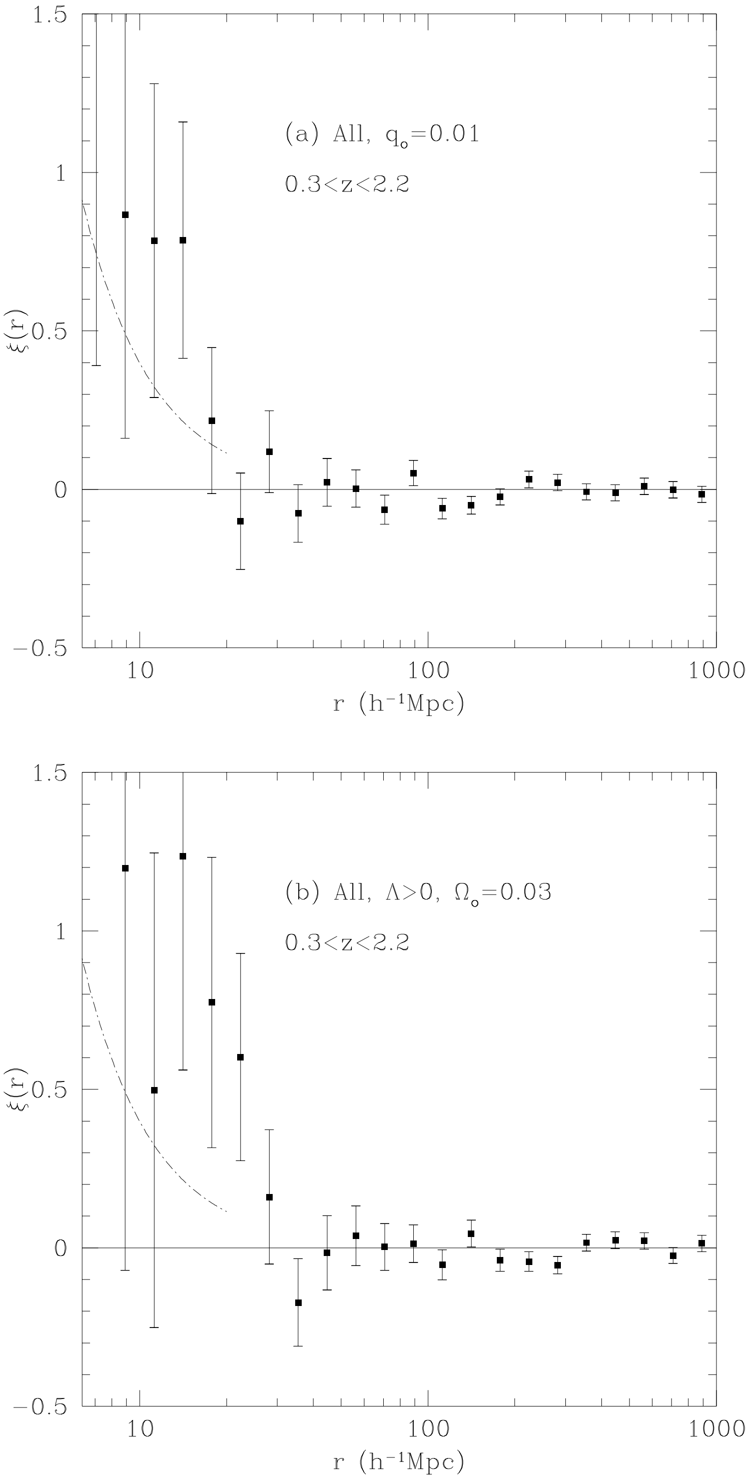

Figure 3.10: The QSO correlation function for the combined sample with (a) $q_0 = 0.01$ and (b) inflationary Λ, $\Omega_0 = 0.03$, $\lambda_0 = 0.97$. For clarity we only plot points excluding the CFHT 'supercluster'. The dot-dashed line is $\xi = (r/6)^{-1.8}$.

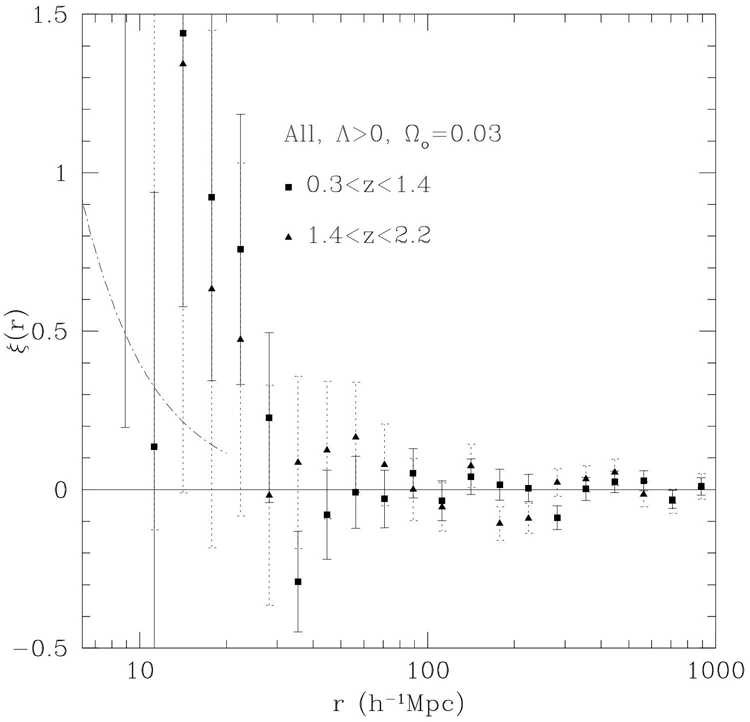

Figure 3.11: The QSO correlation function for $\Omega_0 = 0.03$, $\lambda_0 = 0.97$ in the redshift intervals $0.3 < z < 1.4$ (filled squares) and $1.4 < z < 2.2$ (filled triangles).

In Fig. 3.11 we plot the QSO $\xi(r)$ for $\Omega_0 = 0.03$ and $\lambda_0 = 0.97$ in the two redshift bins used above. From low to high redshift we expect a doubling of the scale of any real feature, if $q_0 = 0.5$ is the correct cosmology. At some level this will be watered down by the angular separation of the QSOs, but all the samples considered in this chapter are of a geometry which is much more extended in the radial direction. There are marginal anti-correlations seen, at $\sim 280\ h^{-1}$ Mpc at low redshift, and at $\sim 200\ h^{-1}$ Mpc at high redshift. Unfortunately these signals are not significant enough to use as convincing 'standard rods'.

To quantify the effect of cosmology (at a somewhat smaller scale), we calculate $\bar{\xi}(25\ h^{-1}$ Mpc) (see Table 3.1). With an inflationary Λ cosmology this quantity is $\bar{\xi}(25) = 0.74 \pm 0.23$, and is larger than for other cosmologies without significant contributions from Λ. We can compare this measurement in the Λ cosmology to a power law with $r_0 = 6\ h^{-1}$ Mpc and slope of -1.8 (making the simplifying assumption that this power law extends to $\sim 25\ h^{-1}$ Mpc). These two correlation functions are inconsistent at the 2.9σ (4σ with CFHT 'supercluster') level. If QSOs randomly sample the galaxy distribution (see arguments below), this is a rejection of the Λ model. This test assumes ξ is approximately stable in comoving coordinates as a function of z. If ξ did in fact evolve faster the rejection would be stronger. Similarly if the power law turned over before $25\ h^{-1}$ Mpc then the present day clustering amplitude would be lower, again increasing the significance of the rejection. The same analysis is attempted for a low q_0 cosmology ($q_0 = 0.01$) but no significant rejection is found.

3.6 The Evolution of QSO Clustering in a Biased Model

At scales of $\sim 10\ h^{-1}$ Mpc the amplitude of the QSO correlation function is such that it is possible to start discriminating between evolutionary models of large-scale structure. In particular, the redshift evolution of the mass correlation function depends strongly on Ω_0. If QSOs are biased with respect to the overall mass distribution, this biasing will also play a major role in the evolution of QSO clustering. SB94 argue that, because the QSO clustering amplitude at high redshift is similar to that of nearby galaxies and Seyferts, QSO clustering evolution is approximately stable in comoving coordinates. This comoving picture is based on the assumption that QSOs, Seyferts and galaxies all have similar clustering properties. However, SB94 do not give any quantitative statements on the cosmological implications of their result. In contrast, Mo & Fang (1993) have used the same data (Durham/AAT and CFHT samples), which give the same clustering result at high redshift, to estimate a large present day correlation length for QSOs compared to the present day galaxy population. They find $r_0(z=0) = (18 \pm 2)\ h^{-1}$ Mpc, by assuming *unbiased* linear theory evolution from the high redshift clustering result; that is $\xi(z) = \xi(0)/(1+z)^2$. This leaves us with a paradox: the high present day amplitude suggests that the QSOs are highly biased with respect to present day galaxies and hence to the mass distribution, yet the result is obtained by assuming that the QSOs are unbiased.

Below, we have constructed a simple and consistent model of QSO clustering evolution, that can be used to compare high redshift QSO clustering and the low z Seyfert clustering amplitude (Georgantopoulos & Shanks, 1994; Boyle & Mo, 1993). To simplify the model we will consider clustering in the linear regime, using the peaks-bias formalism (Bardeen et al., 1986). This formalism is not used in the sense that QSOs are rare, therefore very high peaks, and therefore strongly clustered. It is simply stating that above a given threshold QSOs are able to form, but may only form in a *random fraction* of the peaks that are above that threshold. Bardeen et al (1986) defines the bias parameter b as,

$$b = \frac{\langle\bar{\nu}\rangle}{\sigma(t)} + 1 \tag{3.19}$$

where $\sigma(t)$ is the r.m.s. fluctuation in the mass distribution and $\langle\bar{\nu}\rangle$ defines some threshold above which QSOs/galaxies can form. If we assume that $\langle\bar{\nu}\rangle$ is a constant then the dependence of b on redshift is contained in $\sigma(t)$. This will scale as $\delta\rho/\rho$ and hence for $\Omega_0 = 1$

$$b(z) = (b(0) - 1)(1 + z) + 1 \tag{3.20}$$

This evolution of bias can also be derived using a simple physical model where the QSOs are formed at a specific time by a mechanism which produces biasing and are then allowed to move under the influence of gravity. Fry (1996) shows that, to first order, the galaxy density contrast,

$$\delta_g(\mathbf{x}, t) = \frac{n(\mathbf{x}, t) - \bar{n}}{\bar{n}} \tag{3.21}$$

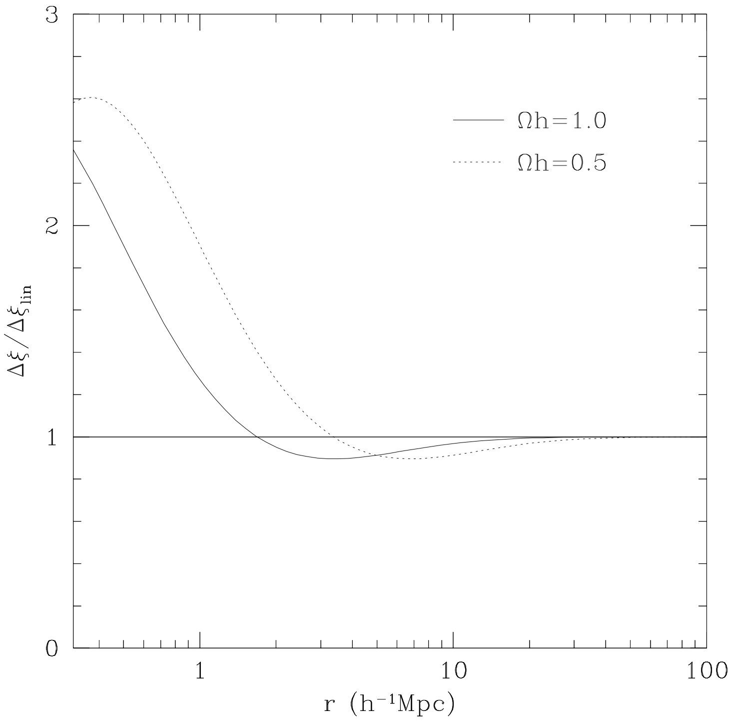

Figure 3.12: Growth of CDM $\bar{\xi}(r)$ for $\Omega_0 = 1$ and $h = 0.5, 1$ in the quasi-linear regime, from $z = 1.27$ to the present. The growth rate is normalized to linear theory evolution, $(1+z)^2$.

satisfies the relation

$$a\frac{\partial \delta_g}{\partial t} = -\theta = a\delta_0 \tag{3.22}$$

where δ_0 is the density contrast (Eq. 1.7) at some initial time, θ is the velocity divergence and a is the cosmological scale factor. Then as the linear bias factor is

$$b(t) = \frac{\delta_g(t)}{\delta(t)} = \frac{\delta_g(t)}{\delta_0 a(t)} \tag{3.23}$$

the solution to Eq. 3.22 shows exactly the same form of evolution as Eq. 3.20.

The average redshift of the combined QSO sample is $\bar{z} = 1.27$. The best comparisons and the tightest constraints will be available from comparing this to clustering at the present day (presently there is no gain from splitting the high redshift QSOs into redshift bins because of the increased errors on the points). We first compare the amplitude of QSO clustering at high redshift to present day galaxy clustering, then go on to make comparisons with the clustering of low redshift Seyfert galaxies. As an estimate of the $z = 0$ galaxy clustering we use $\xi_{\rm gg} = (r/6)^{-1.8}$, which gives $\bar{\xi}_{\rm gg}(10) = 1.00$. This can also be thought of as an estimate of the present mass correlation function, $\xi_{\rho\rho}$, if we include a term for the biasing of galaxies. The QSO correlation function can be related to the mass correlation function via

$$\xi_{\rm qq}(r, z) = [B(1+z)+1]^2 \xi_{\rho\rho}(r, z) \tag{3.24}$$

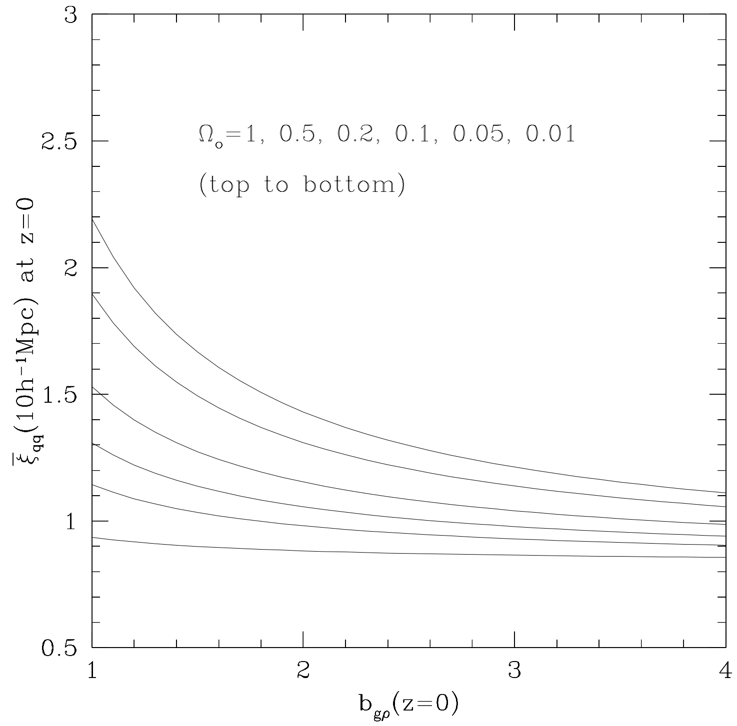

Figure 3.13: Amplitude of $\bar{\xi}_{qq}(10\ h^{-1}\ \mathrm{Mpc})$ at $z = 0$, estimated from the high redshift ($z = 1.27$) QSO clustering amplitude using our biasing model. This is shown as a function of Ω_0 and the present day galaxy bias. It can be seen that both high bias and low Ω_0 reduce the rate of evolution, to give low QSO clustering amplitudes at the present day.

where $B = b(0) - 1$. For $\Omega_0 = 1$

$$\xi_{\rho\rho}(r, 0) = (1 + z)^2 \xi_{\rho\rho}(r, z) \tag{3.25}$$

The biasing of the observed galaxy distribution can be taken into account using

$$\xi_{\mathrm{gg}} = b^2_{\mathrm{g}\rho} \xi_{\rho\rho} \tag{3.26}$$

where $b_{\mathrm{g}\rho}$ is the biasing of the galaxies with respect to the mass at $z = 0$. Combining these equations we obtain an estimate for $b_{\mathrm{q}\rho}$, the estimated present day biasing for QSOs,

$$b_{\mathrm{q}\rho}(z = 0) = B + 1 = \left[\frac{\xi_{\mathrm{qq}}(z)}{\xi_{\mathrm{gg}}(0)}\right]^{1/2} b_{\mathrm{g}\rho} - \frac{1}{1 + z} + 1 \tag{3.27}$$

In the following analysis we will use $\bar{\xi}(10\ h^{-1}\ \mathrm{Mpc})$ as an estimate of the QSO clustering amplitude, which has the advantage of giving a significant signal while at the same time not being affected by large non-linear effects. Hamilton et al (1991) find an empirical fit to the non-linear growth of the CDM correlation function. This is used to predict the deviation away from linear theory expected over the range of scales that we are interested in. Fig. 3.12 shows the relative growth of $\bar{\xi}$ from $z = 1.27$ to $z = 0$ for two CDM type correlation functions ($\Omega_0 = 1$ and $h = 0.5, 1.0$).

Table 3.2: Estimates of $b_{q\rho}$, $\bar{\xi}_{qq}(10)$ and the QSO clustering scale length, r_0, at $z = 0$. These are predicted using our biasing model and $\bar{\xi}(10)$ at $z = 1.27$.

Ω_0	$b_{g\rho}$	$b_{q\rho}(z=0)$	$\bar{\xi}_{qq}(10, z=0)$	$r_0(z=0)$
1	1	1.47 ± 0.16	2.16 ± 0.47	9.23 ± 1.11
1	2	2.38 ± 0.32	1.42 ± 0.38	7.30 ± 1.08
0.1	1	1.27 ± 0.23	1.62 ± 0.57	7.85 ± 1.54
0.1	2	2.31 ± 0.45	1.34 ± 0.52	7.08 ± 1.53
0.02	1	1.09 ± 0.25	1.19 ± 0.54	6.62 ± 1.68
0.2(Λ)	1	1.42 ± 0.29	2.00 ± 0.82	8.84 ± 2.00

The non-linear effects are at the 3 per cent level at 10 h^{-1} Mpc for $h = 1$ and at the 9 per cent level for $h = 0.5$. The CDM correlation function used here is normalized to fit a -1.8 power law at $z = 0$.

So at ~ 10 h^{-1} Mpc the linear approximation is close to the true mass evolution and in particular the error which might be caused by non-linearity is very much smaller than the errors for the QSO clustering amplitude. At smaller scales it would be possible to extrapolate the biasing model and use the non-linear evolution of $\bar{\xi}$ (Hamilton et al., 1991), but to use the linear biasing process at these scales would involve making very large assumptions about the mechanism of biasing, particularly when reaching scales where the clustering is strongly non-linear. The results of this analysis will be much more robust if only the linear regime is considered. Linear theory predictions can also be made in a general case with any value of Ω_0, so instead of $(1 + z)$ there is a general growth factor, $G(z, \Omega_0)$,

$$b_{q\rho}(z=0) = \left[\frac{\bar{\xi}_{qq}(z)}{\bar{\xi}_{gg}(0)}\right]^{1/2} b_{g\rho} - \frac{1}{G(z,\Omega_0)} + 1 \tag{3.28}$$

3.7 Predicted and Observed QSO Clustering at $r \sim 10$ h^{-1} Mpc

We wish to use the above model to find the equivalent present day clustering amplitude for QSOs, which can then be compared to the clustering amplitude of low redshift AGN as well as that of galaxies and other tracers of large-scale structure. Fig. 3.13 shows how the predicted $\bar{\xi}_{qq}(10)$ at $z = 0$ (based on the measured $\bar{\xi}_{qq}(10)$ at $z = 1.27$) varies as a function of $b_{g\rho}$ and Ω_0. Each result will correspond to a value of $b_{q\rho}$. Table 3.2 shows the calculated values of $b_{q\rho}(z = 0)$, $\bar{\xi}_{qq}(10, z = 0)$ and $r_0(z = 0)$ for $b_{g\rho} = 1$ and 2 and various Ω_0. With $\Omega_0 = 1$ and $b_{g\rho} = 1$, the present day QSO bias is $b_{q\rho} = 1.47 \pm 0.16$ but with $b_{g\rho} = 2$ this increases to $b_{q\rho} = 2.38 \pm 0.32$. These correspond to $\bar{\xi}_{qq}(10) = 2.16 \pm 0.47$ and 1.42 ± 0.38 respectively at $z = 0$. Higher

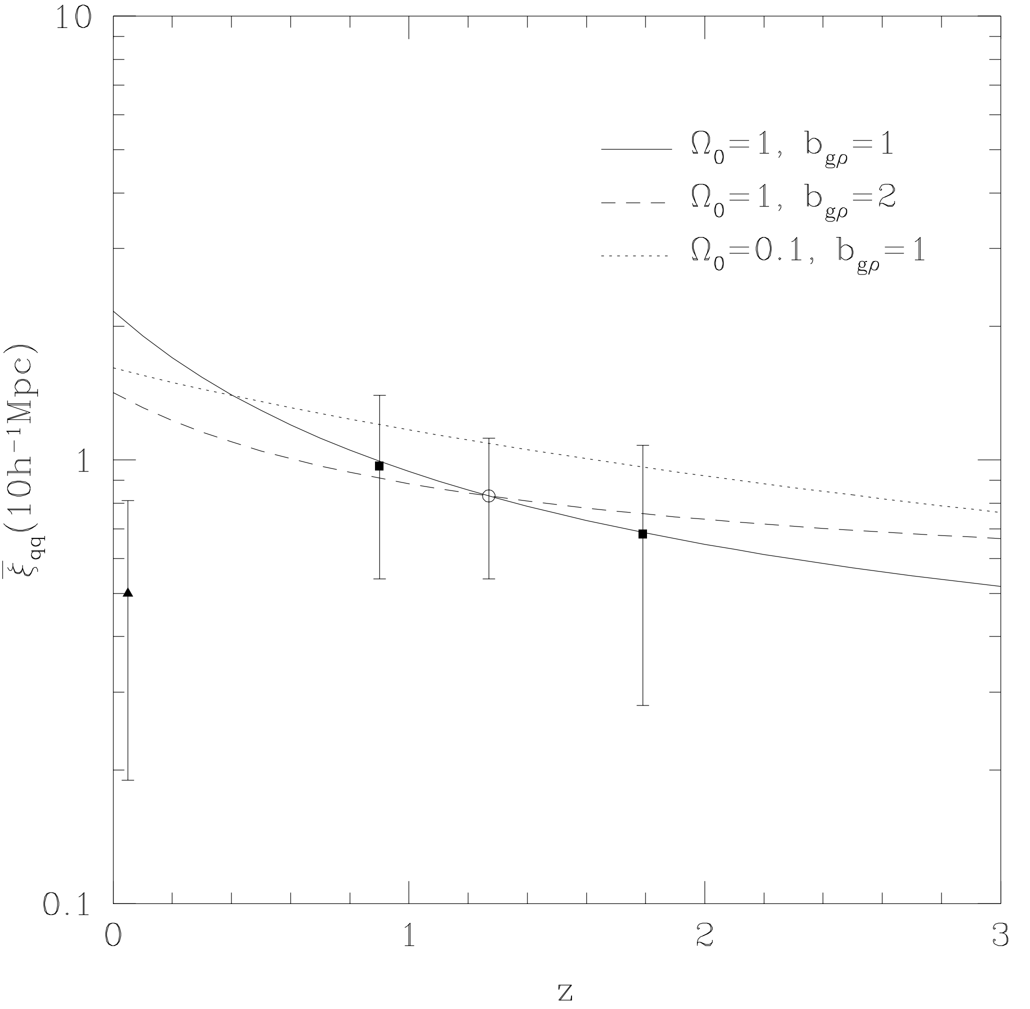

Figure 3.14: The expected evolution in our biasing model for $\Omega_0 = 1$, $b_{g\rho} = 1$ (solid line), $\Omega_0 = 1$, $b_{g\rho} = 2$ (dashed line) and $\Omega_0 = 0.1$, $b_{g\rho} = 1$ (dotted line). The points are the combined QSO clustering result $0.3 < z < 2.2$ (open circle), combined QSO clustering in two redshift bins $0.3 < z < 1.4$ and $1.4 < z < 2.2$ (filled squares), all assuming $\Omega_0 = 1$, and the low redshift AGN clustering amplitude (Georgantopoulos & Shanks 1994; Boyle & Mo 1993) (filled triangle). The $\Omega_0 = 0.1$ model is above the QSO data points as the measured QSO clustering assuming $\Omega_0 = 0.1$ is larger than that found when assuming $\Omega_0 = 1$.

biasing of galaxies (that is, a lower effective mass correlation function) or low Ω_0 reduces the amplitude of $\bar{\xi}_{\mathrm{qq}}(10, z=0)$. Therefore the clustering amplitude of QSOs at the present is a maximum when $\Omega_0 = 1$ and $b_{\mathrm{g}\rho} = 1$. Taking these parameters and assuming a -1.8 power law gives a scale length $r_0(z=0) = 9.23 \pm 1.11\ h^{-1}$ Mpc. This value is obviously significantly smaller than the value of $18 \pm 2\ h^{-1}$ Mpc discussed above (Mo & Fang, 1993); the difference is that we infer a QSO bias with respect to the mass distribution, which produces a slower rate of evolution, while Mo & Fang assume that the QSOs are unbiased. The QSO amplitude lies close to that of the galaxies for all but the $\Omega_0 = 1$, $b_{\mathrm{g}\rho} = 1$ case, and in all cases is significantly lower than the clustering amplitude associated with galaxy clusters, e.g., $r_0 = 14.3 \pm 2.35\ h^{-1}$ Mpc (Dalton et al., 1994).

By making the assumption that AGN at both high and low redshift belong to the same population it is possible to constrain further the evolutionary history of QSOs. Fig. 3.14 compares the clustering amplitude for a combination of the IRAS Seyferts (Georgantopoulos & Shanks, 1994) and EMSS QSOs (Boyle & Mo, 1993) at low redshift, with high redshift QSOs. The low redshift ($z \simeq 0.05$) data have $\bar{\xi}(10) = 0.50 \pm 0.31$. The $\Omega_0 = 1$, $b_{\mathrm{g}\rho} = 1$ model above gives $\bar{\xi}(10) = 2.16 \pm 0.47$ for high z QSOs evolved to the present day and these two values are inconsistent at the 2.9σ level. This then can be interpreted as a rejection of the $\Omega_0 = 1$, $b_{\mathrm{g}\rho} = 1$ scenario. Fig. 3.14 also shows that the $\Omega_0 = 1$, $b_{\mathrm{g}\rho} = 2$ case is only rejected at the 1.9σ level, as the predicted QSO amplitude at $z = 0$ is lower. For $\Omega_0 = 0.1$ and $b_{\mathrm{g}\rho} = 1$ the present day QSO clustering is estimated to be $\bar{\xi}(10) = 1.62 \pm 0.57$ which is only inconsistent with the low z clustering at the 1.7σ level. Therefore the slow evolution of QSO clustering is consistent to better than 2σ with either $\Omega_0 = 1$, $b_{\mathrm{g}\rho} = 2$ or $\Omega_0 = 0.1$, $b_{\mathrm{g}\rho} = 1$.

3.8 The QSO Clustering Amplitude Compared to *COBE* Normalized CDM

Using the combined QSO sample it is also possible to compare the QSO correlation function to the amplitude of CMB fluctuations from *COBE*, using parametric models of the mass correlation function to extrapolate from *COBE* scales to the region between 8 and 50 h^{-1} Mpc. In a sense, we are deriving the QSO bias directly from estimates of the mass fluctuations at very high redshift ($z \sim 1500$), using linear evolution and CDM to relate these fluctuations to our data. In the previous section, we derived values for the QSO bias by making comparisons to low redshift galaxies and Seyferts. We use the $8 - 50\ h^{-1}$ Mpc range, as at this scale, clustering is approximately linear, various different CDM type correlation functions show significant differences and the QSO $\xi(r)$ has relatively small errors. In particular we use the Fourier transform of the generic CDM power spectrum (Efstathiou et al., 1992) which is a good fit to a wide range of cosmologies in the linear regime,

$$P(k) = \frac{Bk}{\{1 + [ak + (bk)^{3/2} + (ck)^2]^{\nu}\}^{2/\nu}} \tag{3.29}$$

where $a = (6.4/\Gamma)\ h^{-1}$ Mpc, $b = (3.0/\Gamma)\ h^{-1}$ Mpc, $c = (1.7/\Gamma)\ h^{-1}$ Mpc, and $\nu = 1.13$. The shape parameter Γ is equivalent to $\Omega_0 h$ for $\Omega_0 = 1$ CDM and flat CDM with a non-zero cosmological constant. The amplitude of the power spectrum, B, is normalized to the *COBE* two year quadrupole, $Q_{\rm rms} = 17.6 \pm 1.5\mu$K (Bennett et al., 1994). To convert this value to the power spectrum amplitude, B, we use the fact that the coefficients for the spherical harmonic expansion of the temperature fluctuations of the CMB are given by,

$$\langle |a_l^m|^2 \rangle = 4\pi^2 \left(\frac{H_0}{c}\right)^4 \left(\frac{\Omega_0}{D_0}\right)^2 \int_0^\infty P(k) j_l^2(kr) \frac{dk}{k^2} \tag{3.30}$$

(Peebles, 1993), where $P(k)$ is the present day power spectrum (Eq. 3.29), j_l is the spherical Bessel function of order l, r is the angular size distance defined in Eq. 3.8 and D_0 is the growth rate of mass perturbations normalized to an Einstein-de Sitter universe at $z = 0$. The comparison of the CDM models to the QSO correlation function is made at a mean redshift of $\bar{z} = 1.27$ so D_0 is replaced with $D(z = 1.27)$. D is a function of z and Ω_0 and is described by

$$D = \left(\frac{x}{x_0}\right)(x^3+1)^{1/2} \int_0^1 \frac{dy}{(1+x^3 y^{6/5})^{3/2}}$$

$$x = \frac{(\Omega_0^{-1} - 1)^{1/3}}{1+z} \tag{3.31}$$

for a universe with zero curvature (Peebles, 1984) (for other cosmologies this is given in Peebles (1980)). Assuming a scale invariant spectrum on *COBE* scales, that is $P(k) = Bk$, then

$$Q_{\rm rms} = \left(\frac{5C_2}{4\pi}\right)^{1/2} T_0 \tag{3.32}$$

where $C_2 = \langle |a_2^m|^2 \rangle$ and $T_0 = 2.735 \pm 0.006$K (Mather et al., 1990), so

$$B = \left(\frac{Q_{\rm rms}}{T_0}\right)^2 \frac{12}{5\pi} \left(\frac{c}{H_0}\right)^4 \left(\frac{D}{\Omega_0}\right)^2 \tag{3.33}$$

Once the power spectrum is normalized, it is a simple process to produce a corresponding $\xi(r)$, via

$$\xi(r) = 4\pi \int_0^\infty k^2 P(k) \frac{\sin(kr)}{kr} dk \tag{3.34}$$

To fit the above models for ξ to the QSO data there are two free parameters, Γ (the shape of $P(k)$) and the QSO bias. For this comparison we will be fitting the QSO data at $z = 1.27$, but will convert the bias measured at this redshift to the value of the QSO bias at the present, using the model described in Section 3.6. The rate of evolution, which is dependent on Ω_0, has to be assumed. Below, two cases are considered, one with $\Omega_0 = 1.0$, the second assuming $\Omega_0 = 0.2$ and $\lambda_0 = 0.8$. We

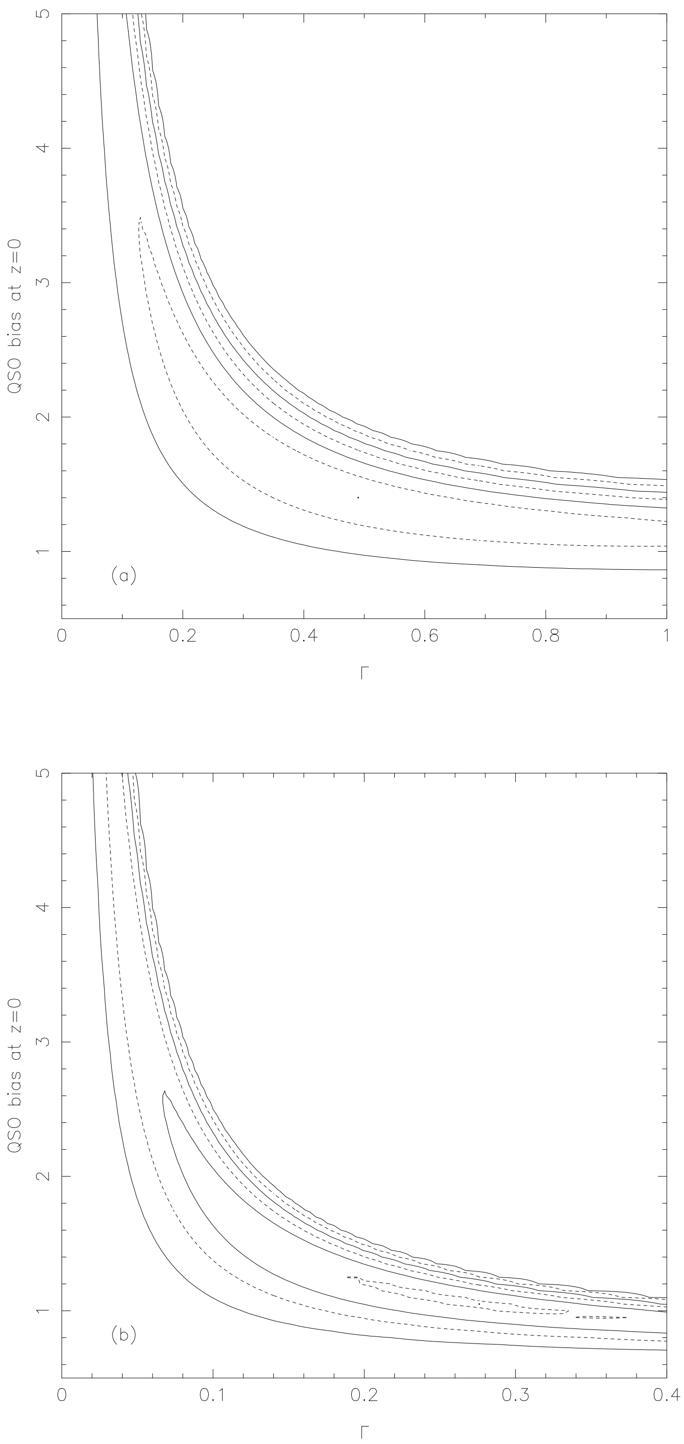

Figure 3.15: Confidence levels for fits of CDM type correlation functions to the combined QSO ξ with free parameters Γ and $b_{q\rho}$ for (a) $\Omega_0 = 1$, and (b) $\Omega_0 = 0.2$, $\lambda_0 = 0.8$. Dotted lines are 0.5σ intervals, solid lines are 1σ intervals.

search the parameter space in Γ and $b_{q\rho}$ to find the set of parameters which best fits the QSO clustering data on scales ~ 8 to $50\ h^{-1}$ Mpc. In all cases we fit the data without the CFHT 'supercluster'.

Fig. 3.15a shows the confidence contours for the $\Omega_0 = 1$ (so $\Gamma \sim h$) case. It is clear that it is not possible, with present statistics, to constrain both the amplitude and shape of the linear correlation function if both are allowed to vary freely. If Γ is constrained to a particular value then a statistically significant result for the bias can be obtained. Taking the value for standard CDM ($\Gamma = 0.5$), the best value of the present day QSO bias is $1.40^{+0.28}_{-0.43}$ and the 3σ upper limit is 1.93.

The same analysis with a different cosmology is shown in Fig. 3.15b which shows the confidence contours and best fit for the case of $\Omega_0 = 0.2$ and $\lambda_0 = 0.8$; here Γ only varies from $0 - 0.4$ (as $\Gamma = 0.2h$). Again, without first fixing one of the two parameters, the range of possible values for both parameters is not well constrained. A currently popular model is CDM with $\Gamma = 0.2$ and a cosmological constant (ΛCDM). Assuming this model, it is possible to obtain $b_{q\rho}(z=0) = 1.2^{+0.13}_{-0.18}$ and a 3σ upper limit of 1.53. In our discussion below we will compare the results found in this section with those of Section 3.6.

3.9 Discussion

3.9.1 Small scale clustering

Assuming a $\gamma = 1.8$ power law the value of $\bar{\xi}(10) = 0.83 \pm 0.29$ (for $\Omega_0 = 1$) implies $r_0 = 5.4 \pm 1.1\ h^{-1}$ Mpc. The best fit power law to the combined QSO data gives $r_0 = 4.00 \pm 1.14\ h^{-1}$ Mpc and $\gamma = 1.59 \pm 0.46$. These results are fully consistent with the present day galaxy value. This also agrees with the value found by Mo & Fang (1993) of $r_0 = 6.6 \pm 0.5\ h^{-1}$ Mpc, but is lower than the Andreani & Cristiani (1992) value of $r_0 \sim 10\ h^{-1}$ Mpc. It is not clear why this last result is higher. Andreani & Cristiani also find little evidence for evolution of clustering in comoving coordinates, consistent with the slow evolution described here.

The natural conclusion from assuming that Seyferts and QSOs come from a similarly clustered population is that their clustering does not evolve in comoving coordinates. The clustering amplitude of both populations is consistent with present day galaxy clustering, which suggests that QSOs randomly sample a comoving galaxy distribution on the scales that have been tested in this analysis, $\sim 10\ h^{-1}$ Mpc. Recent results from the cross-correlation of low redshift EMSS QSOs with APM galaxies (Smith et al., 1995), where the cross-correlation amplitude is found to be similar to the galaxy auto-correlation amplitude, also support the idea that QSOs randomly sample galaxies.

Section 3.6 describes a biasing model to test further the clustering evolution of QSOs. Assuming $\Omega_0 \leq 1$ this model gives an upper limit to the present day clustering of QSOs of $r_0(z=0) = 9.23 \pm 1.11\ h^{-1}$ Mpc. When we postulate that the low redshift Seyferts and the high redshift QSOs are clustered in the same way a strong constraint on the evolution of clustering is obtained, and hence a constraint on a combination of biasing and Ω_0. The case of $\Omega_0 = 1$, $b_{g\rho} = 1$ is ruled out at almost the 3σ level. $\Omega_0 = 1$, $b_{g\rho} = 2$ and $\Omega_0 = 0.1$, $b_{g\rho} = 1$ are consistent to better than 2σ with the QSO evolution. For very low Ω_0 ($\simeq 0.02$) we find consistency to $\sim 1\sigma$. Thus the evolution of QSO clustering over this redshift range seems to imply a low value of Ω_0 or a strongly biased galaxy distribution (and therefore a biased QSO distribution). It is difficult to argue that QSOs can be strongly biased compared to normal galaxies. The above biasing model shows that as biasing is increased, the rate of evolution is reduced, forcing the QSOs to have a similar amplitude to galaxies at the present time. A similar level of biasing is then required for both galaxies and QSOs.

3.9.2 Intermediate scale clustering

The QSO ξ is compared to a correlation function produced via a Fourier transform of the generic CDM power spectrum (Efstathiou et al., 1992) normalized to the CMB results from the two-year *COBE* data (Bennett et al., 1994). Because the shape of our correlation function is not well constrained, we are effectively comparing the QSO clustering amplitude to the CMB anisotropy amplitude. To do this we use a linear model power spectrum to extrapolate from *COBE* scales, to scales where we have a QSO clustering signal ($\sim 8 - 50\ h^{-1}$ Mpc). *COBE* normalized standard CDM, with $\Omega_0 = 1$ and $\Gamma = 0.5$, gives a best fit of $b_{q\rho}(z=0) = 1.40^{+0.28}_{-0.43}$; while for CDM plus a cosmological constant, $\Omega_0 = 0.2$, $\lambda_0 = 0.8$ and $\Gamma = 0.2$ we find $1.20^{+0.13}_{-0.18}$. The 3σ upper limits for these two models are 1.93 and 1.53 for standard CDM and ΛCDM respectively. From these values of the QSO bias we can calculate a present day QSO clustering amplitude, with which to compare the results found in Section 3.6, $\bar{\xi}(10, z=0) = 2.30^{+1.87}_{-1.22}$ and $\bar{\xi}(10, z=0) = 3.54^{+2.80}_{-2.46}$ for standard CDM and ΛCDM respectively. These values are higher than the low redshift AGN clustering result ($\bar{\xi}(10, z \simeq 0) = 0.50 \pm 0.31$), although the increased errors result in no significant inconsistency with the low redshift clustering of the AGN, or the $z = 0$ clustering of QSOs estimated from our biasing models.

Thus the fits to the intermediate scale QSO correlation function (at $z = 1.27$) prefer a low bias for $\Omega_0 = 1$ CDM with $\Gamma = 0.5$. This is in contrast to the small scale evolution results of Section 6 where a high bias is required for the $\Omega_0 = 1$ case. These data might be taken as evidence for low Ω_0, but the errors are still large, and there exists a narrow range where the two bias estimators overlap for $\Omega_0 = 1$. For ΛCDM we find a similar result, which also suggests fast evolution of clustering, again in contradiction (although not significantly) to the small scale evolution results. These results show that new surveys, such as the 2-degree Field QSO survey are vitally important, in order to reduce the large errors that exist presently.

3.9.3 Large scale clustering

The addition of the LBQS survey to the data used in Shanks & Boyle (1994) greatly increases our statistics at large scales, as the number of pairs per bin in the LBQS becomes greater than in the Durham/AAT sample at scales $> 100\ h^{-1}$ Mpc. On these scales the combined sample has errors of ± 0.025. This can be compared to previous estimates, for example, $\pm 0.1 - 0.15$ for a sample of 125 QSOs at $1.5 < z < 3.0$ (Osmer & Hewett, 1991). Looking at the region at $40 - 100\ h^{-1}$ Mpc, where an anti-correlation was seen in the Durham/AAT sample, there is no evidence that the LBQS (and similarly the CFHT and ESO/AAT surveys) shows this signal on these scales. The Durham/AAT is still found to have a negative signal in this region, in particular at $\simeq 89\ h^{-1}$ Mpc. A direct comparison between the LBQS and Durham/AAT samples produces a 2σ inconsistency at scales $40 - 100\ h^{-1}$ Mpc.

A combined sample of all surveys for $0.3 < z < 2.2$ gives us a ξ which is to first order consistent with a Poisson distribution on all scales larger than $40\ h^{-1}$ Mpc. There is a marginal signal at $\sim 100\ h^{-1}$ Mpc which could be tested by larger samples. The errors at large scales are such that we can provide the most accurate measurements of large-scale structure available at $> 100\ h^{-1}$ Mpc from redshift survey data.

Changing our assumed cosmology, some changes are seen in the correlation function. For $q_0 = 0.01$ the negative region at $\simeq 89\ h^{-1}$ Mpc moves out past $100\ h^{-1}$ Mpc and similarly for the $\Omega_0 = 0.03$, $\lambda_0 = 0.97$ case, this moves to $\sim 200\ h^{-1}$ Mpc. The Λ model, if incorrect, should be rejected by the change of scale of linear features in the correlation function. There are negative regions in the correlation function for this cosmology in both low and high redshift bins, but these features are at low signal to noise and do not appear to correspond to the same scale.

We compare the QSO clustering amplitude, $\bar{\xi}(25)$, in a cosmology with a cosmological constant, $\Omega_0 = 0.03$, $\lambda_0 = 0.97$, to a power law with $\gamma = 1.8$ and $r_0 = 6\ h^{-1}$ Mpc. These are inconsistent at the 2.9σ level. In this cosmology the linear growth rate from $z = 1.27$ to $z = 0.0$ is low, only a factor of 1.26, compared to 2.27 for $\Omega_0 = 1$. Therefore the evolution is approximately stable in comoving coordinates. So, if QSOs do randomly sample the galaxy distribution then this result rejects the above cosmology with a large cosmological constant.

3.10 Conclusions

We have analysed a total sample of > 1500 QSOs with $0.3 < z < 2.2$. In particular we have looked at the clustering in the LBQS survey and used a simple but self consistent model for biased clustering evolution. From this analysis the following conclusions can be drawn:

1. At small scales there is a marginal detection of clustering in the LBQS; $\bar{\xi}(10) =$

1.86 ± 1.28 (assuming $\Omega_0 = 1$). With $\Omega_0 = 0.1, 0.02$ and cases with cosmological constants there is no significant clustering in the LBQS. The combined sample has $\bar{\xi}(10) = 0.83 \pm 0.29$ for $\Omega_0 = 1$ (including re-analysed CFHT and ESO/AAT data). The results for other cosmologies are shown in Table 3.1. The LBQS is not an efficient sample to use for clustering at this scale due to its sparsely sampled nature.

2. At large scales the LBQS makes a significant contribution to clustering statistics. The LBQS does not support the anti-correlation found in the Durham/AAT survey at scales $40 - 100\ h^{-1}$ Mpc by SB94, but is only inconsistent at the 2σ level. At $> 100\ h^{-1}$ Mpc the upper limit on a detected signal is now at the ± 0.025 level, which constitutes the best limit so far on the homogeneity of the Universe on large scales (other than measurements from CMB experiments).

3. A model for biased clustering evolution based on the peaks-bias formalism (Bardeen et al., 1986) was used to derive a present day clustering amplitude for QSOs. In the case of $\Omega_0 = 1$ with an unbiased galaxy distribution, $\bar{\xi}(10) = 2.16 \pm 0.47$ for QSOs at $z = 0$. Assuming a -1.8 power law this is equivalent to $r_0 = 9.23 \pm 1.11$. If Ω_0 is decreased or galaxy biasing is increased this value will decrease. Hence this value of r_0 is an upper limit on the present day QSO clustering amplitude. This value is significantly lower than the clustering amplitude of rich galaxy clusters, and lower than a value for the present day clustering of QSOs calculated by Mo & Fang (1993) using evolution that assumes that QSOs trace the mass distribution.

4. If the low redshift AGN population and the high redshift QSO population are both clustered in the same way, then the clustering evolution is best fit by a slowly evolving model. The $\Omega_0 = 1$, unbiased galaxies model (see above) is then inconsistent with the clustering evolution at the $\sim 3\sigma$ level. The slow development of QSO clustering therefore implies low Ω_0 and/or high biasing.

5. Comparing the QSO ξ to linear theoretical predictions of CDM correlation functions, normalized to the CMB anisotropy (Bennett et al., 1994) with two free parameters (biasing and Γ), it is not possible to obtain a significant constraint on QSO biasing. Assuming a value of Γ this does become possible. For $\Omega_0 = 1$, $\Gamma = 0.5$ (standard CDM), $b_{q\rho}(z = 0) = 1.40^{+0.28}_{-0.43}$. For $\Omega_0 = 0.2$, $\lambda_0 = 0.8$, $\Gamma = 0.2$ (ΛCDM) the value found is $1.20^{+0.13}_{-0.18}$.

6. For a flat cosmology with $\lambda_0 = 0.97$, $\Omega_0 = 0.03$, the amplitude at $25\ h^{-1}$ Mpc is $\bar{\xi}(25) = 0.74 \pm 0.23$. This is inconsistent with $\xi = (r/6)^{-1.8}$ at the 2.9σ level, confirming the result obtained in Shanks & Boyle (1994). Assuming that high redshift QSOs randomly sample the galaxy population, this is a significant rejection of this inflationary $\Lambda > 0$ cosmology.

The small scale evolution and intermediate scale comparisons to the CMB (via CDM) could be used to imply low Ω_0. However, the data allow a range of acceptable values for bias in $\Omega_0 = 1$ CDM around $b_{q\rho} \simeq b_{g\rho} \simeq 2$. With the advent of new QSO samples with order of magnitude improvements in numbers, a combination of small scale evolution and comparison to the CMB will give us a great opportunity to independently discriminate between different values of biasing and Ω_0. For example, measuring the QSO power spectrum to *COBE* scales and comparing it to anisotropy in the CMB will give a direct measurement of QSO bias.